Development and Dissipation of Ca^{2+} Gradients in Adrenal Chromaffin Cells

Fernando D. Marengo and Jonathan R. Monck
Department of Physiology, UCLA School of Medicine, Los Angeles, California 90095 USA

ABSTRACT We used pulsed laser imaging to measure the development and dissipation of Ca^{2+} gradients evoked by the activation of voltage-sensitive Ca^{2+} channels in adrenal chromaffin cells. Ca^{2+} gradients appeared rapidly (<5 ms) upon membrane depolarization and dissipated over several hundred milliseconds after membrane repolarization. Dissipation occurred with an initial fast phase, as the steep gradient near the membrane collapsed, and a slower phase as the remaining shallow gradient dispersed. Inhibition of active Ca^{2+} uptake by the endoplasmic reticulum (thapsigargin) and mitochondria (carbonylcyanide *p*-trifluoro-methoxyphenylhydrazone/oligomycin) had no effect on the size of Ca^{2+} changes or the rate of gradient dissipation, suggesting that passive endogenous Ca^{2+} buffers are responsible for the slow Ca^{2+} redistribution. We used a radial diffusion model incorporating Ca^{2+} diffusion and binding to intracellular Ca^{2+} buffers to simulate Ca^{2+} gradients. We included a 3D optical sectioning model, simulating the effects of out-of-focus light, to allow comparison with the measured gradients. Introduction of a high-capacity immobile Ca^{2+} buffer, with a buffer capacity on the order of 1000 and appropriate affinity and kinetics, approximated the size of the Ca^{2+} increases and rate of dissipation of the measured gradients. Finally, simulations without exogenous buffer suggest that the Ca^{2+} signal due to Ca^{2+} channel activation is restricted by the endogenous buffer to a space less than 1 μm from the cell membrane.

INTRODUCTION

The elevation of cytosolic free Ca^{2+} concentration regulates many cellular processes. Ca^{2+} triggers dense-core granule exocytosis in neuroendocrine cells, synaptic vesicle fusion in neurons, and contraction in muscle. Ca^{2+} also regulates hormone-induced changes in glucose metabolism, oxidative phosphorylation in mitochondria, and transcription in the nucleus. Given these many roles, Ca^{2+} ought to be compartmentalized so that all these processes are not all activated alike. In addition to compartmentalization in different organelles, Ca^{2+} gradients provide a means of compartmentalizing Ca^{2+} signals in the cytosol. As a result, intracellular Ca^{2+} signals may be regulated spatially and temporally.

In neuroendocrine cells, such as adrenal chromaffin cells, the trigger for exocytosis is a localized Ca^{2+} increase near the cell membrane that develops after the activation of voltage-dependent Ca^{2+}channels (O'Sullivan et al., 1989; Neher and Augustine, 1992; Monck et al., 1994). Exocytosis was found to be more prominent when the Ca^{2+} increase resulted from Ca^{2+}entry through Ca^{2+} channels rather than Ca^{2+} release from intracellular stores (Kim and Westhead, 1989; O'Sullivan et al., 1989; Augustine and Neher, 1992), and the spatially averaged Ca^{2+} measured during depolarizing stimuli is considerably lower than the Ca^{2+} concentrations required to trigger comparable rates of exocytosis when the Ca^{2+} is delivered uniformly, either via the patch pipette or by photolysis of caged compounds (Augustine and Neher, 1992; Neher and Zucker, 1993). In addition to vesicle fusion, Ca^{2+} regulates other exocytotic processes that respond to different Ca^{2+} concentrations with different temporal characteristics. For example, Ca^{2+} may be involved in vesicle translocation between different pools, facilitation of secretion during repetitive stimuli (Seward and Nowycky, 1996; Neher and Zucker, 1993; Neher, 1998), and endocytosis (Engisch and Nowycky, 1998). Furthermore, different pathways of regulated exocytosis with distinct kinetics and Ca^{2+} sensitivity may exist in chromaffin cells (Seward and Nowycky, 1996; Seward et al., 1996). Characterization of the temporal and spatial properties of Ca^{2+} gradients is, therefore, necessary to understand the regulation of stimulus-induced exocytosis. However, because of the difficulties involved in measuring Ca^{2+} with high spatial and temporal resolution, there is little experimental information on the properties of Ca^{2+} gradients.

An alternative approach to experimental measurements is to use mathematical models to simulate the Ca^{2+} gradients that might be generated after Ca^{2+} entry through channels, Ca^{2+} diffusion, and binding to intracellular Ca^{2+} buffers (Smith and Zucker, 1980; Connor and Nikolakapoulou, 1982; Zucker and Stockbridge, 1983; Chad and Eckert, 1984; Simon and Llinás, 1985; Neher, 1986). For example, a radial diffusion model has been used to simulate the Ca^{2+} gradients that would be generated on opening of Ca^{2+} channels in small spherical cells (Sala and Hernández-Cruz, 1990; Nowycky and Pinter, 1993). These studies have provided considerable information on possible types of Ca^{2+} gradients. However, a major problem inherent to this approach is the appropriate selection of concentrations, affinities, and kinetic rate constants for the endogenous Ca^{2+} buffers. Recent studies in patch-clamped adrenal chromaffin cells have estimated a buffer capacity, defined as the ratio of the change in Ca^{2+}-buffer complex concentration

Received for publication 10 December 1999 and in final form 5 July 2000.
Address reprint requests to Dr. Jonathan R. Monck, Department of Physiology, Center for Health Sciences, 53-263, UCLA School of Medicine, 10833 Le Conte Avenue, Los Angeles, CA 90095. Tel.: 310-825-0932; Fax: 310-206-3788; E-mail: jrmonck@mednet.ucla.edu.

0006-3495/00/10/1800/21 $2.00

over the change in free Ca^{2+} concentration, of 40–90 by measuring the changes in free Ca^{2+} and Ca^{2+} bound to exogenous buffer (Neher and Augustine, 1992; Zhou and Neher, 1993). A further study using photolytic release of "caged Ca^{2+} " concluded that adrenal chromaffin cells contain ~4 mM of a low-affinity (K_d = 100 μM) endogenous Ca^{2+} buffer (Xu et al., 1997).

The dynamics of Ca^{2+} redistribution after Ca^{2+} entry is influenced by the presence of fixed and mobile Ca^{2+} buffers (Nowycky and Pinter, 1993). As a result the temporal and spatial properties of Ca^{2+} gradients can be used to determine the properties of endogenous Ca^{2+} buffers. In this study, we have measured the development and dissipation of Ca^{2+} gradients, using pulsed laser Ca^{2+} imaging (Monck et al., 1994), and compared the measured Ca^{2+} gradients with gradients simulated with a radial diffusion model. We were able to resolve the presence of Ca^{2+} gradients from very early times (<5 ms) during a depolarizing stimulus to several hundred of milliseconds afterward. We also show that inhibition of intracellular Ca^{2+} stores does not alter Ca^{2+} gradient development or dissipation. To our knowledge, this is the first detailed experimental characterization of the development and dissipation of Ca^{2+} gradients in adrenal chromaffin cells. Based on these data, we predict the properties of the endogenous Ca^{2+} buffer and the pattern of Ca^{2+} gradients in the absence of exogenous Ca^{2+} buffers (e.g., indicators). Our next step is to relate the spatial and temporal properties of the intracellular Ca^{2+} signal to the regulation of exocytosis.

MATERIALS AND METHODS

Cell preparation and solutions

Chromaffin cells were prepared from bovine adrenal medullae by enzymatic digestion (Burgoyne et al., 1988). Isolated cells were resuspended in Dulbecco's modified Eagles medium supplemented with 10% fetal calf serum, 8 μM fluorodeoxyuridine, 50 μg/ml gentamycin, 10 μM cytosine arabinofuranoside, 2.5 μg/ml fungizone, 25 U/ml penicillin, and 25 μg/ml streptomycin. Cells were plated at a density of 100,000 cells/ml on glass-bottomed chambers and kept for 1–4 days in culture before use. For experiments, chromaffin cells were washed in an extracellular medium comprising 120 mM NaCl, 20 mM Hepes, 4 mM $MgCl_2$, 5 mM $CaCl_2$, 5 mg/ml glucose, and 1 μM tetrodotoxin (pH 7.25). The standard internal solution used in the patch-clamp pipettes contained 125 mM Cs D-glutamate, 30 mM Hepes, 8 mM NaCl, 1 mM $MgCl_2$, 2 mM Mg-ATP, 0.3 mM GTP, and 0.3 mM Cs-EGTA (pH 7.2). The Ca^{2+} indicators rhod-2 (triammonium salt) and Oregon Green 1,2-bis(2-aminophenoxy)ethane-*N,N,N,N*-tetraacetic acid-5N (OGB-5N) were added to the pipette solution at 0.2 mM and 0.3 mM, respectively. These solutions allow measurement of Ca^{2+} currents because Na^+ and K^+ currents are prevented. The holding potentials have not been corrected for junction potentials (Neher, 1992).

Measurement of Ca^{2+} gradients with pulsed laser imaging

Ca^{2+} gradients were measured using pulsed laser Ca^{2+} imaging of whole-cell patch-clamped cells (Monck et al., 1994). The imaging system consists of an inverted epifluorescence microscope (model IX-70; Olympus), a Peltier-cooled charge-coupled device (CCD) camera (model PXL; Photometrics, Tucson, AZ) with a 1317 × 1035 pixel CCD chip (model KAF 1400; Kodak), and a host Pentium microcomputer. Illumination is achieved with a high-intensity pulsed coaxial flash lamp dye laser (LumenX model LS-1400; Phase-R Corporation, New Durham, NH), which provides short (350 ns) high-intensity pulses of illumination (Kinosita et al., 1988). A patch-clamp setup, comprising a patch-clamp amplifier (model Axopatch 200A; Axon Instruments, Foster City, CA) and a data acquisition interface (model IDA15125; Indec Systems, Mountain View, CA), was used for voltage-clamp recording and precise synchronization of the laser pulses with the Ca^{2+} currents. The laser light is focused into a multimode fiber optic (1-mm-diameter silica, 0.47 N.A.; General Fiber Optics Corporation, Fairfield, NJ). The other end of the fiber optic is coupled to the epifluorescence port of the microscope, using a custom-built adapter containing a fused silica plano-convex lens (1-inch diameter, F/2; Oriel Corporation, Stratford, CT) positioned ~2 inches from the end of the fiber optic. This arrangement results in global illumination of the microscope field of view.

For Ca^{2+} measurements with the Ca^{2+} indicator rhod-2 (Minta et al., 1989), we use coumarin 525 (0.02 mM in methanol) as the lasing dye, which gives an appropriate emission spectrum (500–540 nm) for the excitation of rhod-2. The epifluorescence filter block contains a 570-nm dichroic mirror and 585 nm long pass emission filter (Chroma Optical, Brattleboro, VT). A high-numerical-aperture objective (N.A. 1.4, plan apo 60×; Olympus America, Melville, NY) was used to image the cells. After allowing 10 min for the Ca^{2+} indicator to diffuse into the cell, fluorescence measurements were taken as image pairs: a control image with no depolarization (i.e., constant holding potential) and a stimulus image with a depolarizing step pulse. The results are shown as ratio images of the stimulus image divided by the corresponding control image. Taking the ratio of the images in this way corrects for spatial differences in cell thickness (light path length), indicator concentration, and accessible cytosolic volume (Bright et al., 1989). Pairing of the control and stimulus images minimizes the effects of cell movements. The ratio images (F_t/F_0) are used to analyze the gradients and to estimate the free Ca^{2+} concentrations as described below.

Estimation of Ca^{2+} concentration

The ratio of the stimulus image divided by the control image is displayed as a pseudocolor image representing the fractional change in fluorescence. Because the ratio corrects for differences in indicator concentration, indicator excluded volume, and light path length, the images showing the fractional change in fluorescence represent spatial maps of the Ca^{2+} changes, provided that the cell does not move between the control and stimulus images. Rhod-2 does not undergo a shift in either excitation or emission spectra on binding Ca^{2+} (Minta et al., 1989), so we cannot use a ratiometric calibration scheme (Grynkiewicz et al., 1985). Instead, the change in Ca^{2+} concentration was estimated from the fractional fluorescence change (stimulus/control ratio, F_t/F_o), as described previously (Monck et al., 1988, 1994). We used a value of 1880 nM for the K_d (Escobar et al., 1997) and 0.013 for α (the ratio of the fluorescence of free and Ca^{2+} bound rhod-2, determined in vitro, using internal solutions with "zero" Ca^{2+} (10 mM EGTA) and saturating Ca^{2+}, respectively). Assuming a value of 100 nM for the resting Ca^{2+} concentration, these values give an estimated peak Ca^{2+} concentration of ~200–250 nM at the end of a 40-ms depolarizing stimulus. There are some caveats regarding the conversion to Ca^{2+}, as we do not know the precise value of the resting Ca^{2+} or the in situ calibration for the indicator dyes. However, attempts to saturate rhod-2 in situ, using ionomycin, gave F_t/F_o values of >8, which indicates that the resting Ca^{2+} concentration was less than 200 nM. Estimates of the Ca^{2+} change, using different resting free Ca^{2+} concentrations in the range of 50–200 nM, give peak Ca^{2+} increases of ~2–2.5 times the resting concentration. The Ca^{2+} concentration estimates are relatively insensitive to the value of α used, because the amounts of Ca^{2+}-indicator complex are

small (~5–10%). Thus, provided the in situ value of α is less than 0.05, the estimates of Ca^{2+} remain accurate. In addition, the Ca^{2+} calibration procedure assumes equilibrium conditions, and during the Ca^{2+} current the Ca^{2+} indicators will not be at equilibrium with the free Ca^{2+} ions. Therefore, we chose to express most of the data as the fractional fluorescence change (F_t/F_o), as this best represents the measured parameter.

Analysis of Ca^{2+} gradients

Ratio images representing the fractional fluorescence change (F_t/F_o) are used to display the spatial distribution of Ca^{2+} concentration. The ratios are made after a 3 × 3 kernel is averaged for each pixel in the original fluorescence images. Thus, each averaged region corresponds to a square with sides three times the measured pixel size of 113 nm, or 339 nm. To analyze the Ca^{2+} gradients we used cross-sectional profiles through the center of the cell. The value chosen for each position in the profile was taken with no further averaging. The focus of the cell was always chosen as the image with the maximum visible diameter, which in a perfectly spherical cell would represent a section through the center of the cell. To maximize the signal available for analysis, the direction of the profile was usually chosen from the brightest point around the periphery through the center of the cell. However, we tried to avoid the regions beneath the pipette (at 2–4 o'clock in the displayed images), as these were often distorted by the presence of either out-of-focus light or reflected light from the pipette. In some cells the nucleus was visible in the plane of focus. If the profile was drawn through the nucleus we observed an inflection in the profile shape, which presumably occurs because the nucleus membrane provides a significant barrier for diffusion (see Naraghi et al., 1998). To prevent this from affecting the analysis, we avoided analyzing profiles through the nucleus. Fortunately, the nucleus was usually displaced from the center of the cell. In most cells the nucleus was below the plane of focus, and in other cells it was displaced to the side, so we could still select a profile to the center of the cell while avoiding the nucleus.

Mathematical model for Ca^{2+} entry, diffusion, and buffering

To simulate the changes in the concentration of free Ca^{2+} and other species (e.g., free buffers and buffer-Ca^{2+} complexes) as a function of time and radial distance, we developed a radial diffusion model. This model assumes a uniform entry of Ca^{2+} through Ca^{2+} channels in a spherical cell; it is based on the model of Nowycky and Pinter (1993).

The partial differential equation describing the change in concentration of a diffusible species is

$$\frac{\partial[S]}{\partial t} = D_S\left(\frac{\partial^2[S]}{\partial r^2} + \frac{2}{r}\frac{\partial[S]}{\partial r}\right) \quad (1)$$

where [S] is the concentration of the diffusible species, S; r is the radial distance, and D_S is the diffusion coefficient (Crank, 1975). This equation can be used to describe the diffusion of Ca^{2+} and various Ca^{2+} buffers.

The cell is modeled as a sphere composed of concentric shells of equal thickness (0.1 μm). A simplifying assumption is that each shell represents a well-mixed system and that diffusion within the shell can be neglected. Diffusion of Ca^{2+} and buffers is assumed to occur solely at the shell interfaces and can be described by a function involving the shell thickness (i.e., diffusional distance), shell surface areas (inner and outer), and the diffusion coefficient. Given these assumptions, Eq. 1 can be represented as a system of first-order, ordinary differential equations describing the concentration of Ca^{2+} (and other diffusible species) in each shell. We follow the convention used by Nowycky and Pinter (1993), where the first shell is the outer shell and the Nth shell is the innermost shell. For the ith shell of N shells, the diffusion equation takes the form

$$\frac{d[Ca^{2+}]}{dt} = \frac{D_{Ca}}{V_i\delta}$$
$$(A_{i-1}([Ca^{2+}]_{i-1} - [Ca^{2+}]_i) - A_i([Ca^{2+}]_i - [Ca^{2+}]_{i+1})) \quad (2)$$

where $[Ca^{2+}]_i$ is the concentration of free Ca^{2+} in the ith shell, D_{Ca} is the diffusion coefficient for Ca^{2+}, δ is the shell thickness, V_i is the shell volume, and A_i and A_{i-1} are the surface areas of the inner and outer surfaces of the ith shell. The boundary conditions specify that diffusion does not occur across the outermost spherical boundary or out of the innermost shell, which is spherical. Computationally, this was achieved by setting A_0 (outer boundary of first shell) and A_N (inner boundary of Nth shell) to zero.

Ca^{2+} leak and extrusion across the plasma membrane

The active extrusion from the cell was assumed to be solely via a Ca^{2+}-ATPase, which was modeled assuming Michaelis-Menten kinetics (Sala and Hernández-Cruz, 1990). The rate of change of Ca^{2+} in the outermost shell due to extrusion by the Ca^{2+}-ATPase is given by the expression

$$\left(\frac{d[Ca^{2+}]}{dt}\right)_{Ex} = \frac{-V_{max}A_1[Ca^{2+}]_1}{V_1([Ca^{2+}]_1 + K_m)} \quad (3)$$

where V_{max} and K_m are, respectively, the maximum pumping rate and the Michaelis-Menten constant for the Ca^{2+}-ATPase. To provide a steady-state Ca^{2+} concentration in the absence of Ca^{2+} entry through Ca^{2+} channels, a constant leak was defined as being equal and opposite to the Ca^{2+} extrusion by the Ca^{2+}-ATPase at the resting Ca^{2+} concentration, calculated using Eq. 3.

Calcium entry through Ca^{2+} channels

The rate of change in free Ca^{2+} concentration in the first shell due to Ca^{2+} influx is defined by

$$\left(\frac{d[Ca^{2+}]}{dt}\right)_{In} = \frac{I_{Ca}}{2FV_1}\cdot(1 - e^{-t_{Ca}/\tau}) \quad (4)$$

where I_{Ca} is the inward Ca^{2+} current, F is Faraday's constant, V_1 is the volume of the first shell, t_{Ca} is the time after initiation of the depolarization, and τ is the time constant for Ca^{2+} current activation.

Ca^{2+} binding to endogenous and exogenous Ca^{2+} buffers

The rate of change of Ca^{2+} due to binding to Ca^{2+} buffer X is given by the expression

$$\left(\frac{d[Ca^{2+}]}{dt}\right)_{B^x} = -\left(\frac{d[CaB^x]}{dt}\right)$$
$$= k_{-1}[CaB^x]_i - k_{+1}[Ca^{2+}]_i[B^x]_i \quad (5)$$

where $[CaB^x]$ is the concentration of Ca^{2+} bound to buffer X, $[B^x]$ is the concentration of unbound buffer, and k_{+1} and k_{-1} are, respectively, the forward and reverse rate constants for the binding of Ca^{2+} to the buffer. The model considers five Ca^{2+} buffers, denoted B^A through B^E, where B^A, B^B, and B^C are used for various endogenous buffers, B^D represents the indicator dye, and B^E represents the EGTA added to the pipette solutions.

Final model

From Eqs. 2–5, we can define a first-order differential equation to describe the change in Ca^{2+} concentration in each shell:

$$\frac{d[Ca^{2+}]}{dt} = \frac{D_{Ca}}{V_i\delta}(A_{i-1}([Ca^{2+}]_{i-1} - [Ca^{2+}]_i) - A_i([Ca^{2+}]_i - [Ca^{2+}]_{i+1})) + \left(\frac{d[Ca^{2+}]_i}{dt}\right)_{B^A} + \left(\frac{d[Ca^{2+}]_i}{dt}\right)_{B^B} + \left(\frac{d[Ca^{2+}]_i}{dt}\right)_{B^C} + \left(\frac{d[Ca^{2+}]_i}{dt}\right)_{B^D} + \left(\frac{d[Ca^{2+}]_i}{dt}\right)_{B^E} + \left(\frac{d[Ca^{2+}]_i}{dt}\right)_{I_{Ca}} + \left(\frac{d[Ca^{2+}]_i}{dt}\right)_{Leak} + \left(\frac{d[Ca^{2+}]_i}{dt}\right)_{Pump} \quad (6)$$

The last three terms, for Ca^{2+} influx, leak, and extrusion, are only present in the outer shell, i.e., they are zero when $i \neq 1$. A set of similar equations can be developed for the change in the concentration of Ca^{2+}-buffer complex for each buffer:

$$\frac{d[CaB^x]}{dt} = \frac{D_x}{V_i\delta}(A_{i-1}([CaB^x]_{i-1} - [CaB^x]_i) - A_i([CaB^x]_i - [CaB^x]_{i+1})) + \left(\frac{d[CaB^x]_i}{dt}\right) \quad (7)$$

$$[B^x]_i = [B^x_{total}]_i - [CaB^x]_i \quad (8)$$

We make the additional assumption that the diffusion coefficients for Ca^{2+}-buffer complex and unbound buffer are equal, so that the total concentration of buffer in each shell is constant and equal to the initial total concentration of buffer. This assumption eliminates the need to have a set of equations for the change in concentration of unbound buffer. Note that for fixed, immobile buffers D_x is set to zero.

Equations 6–8 were numerically integrated using a first-order Euler algorithm written in Visual Basic 5.0 (Microsoft Corp., Redmond, WA). The output of the simulation was verified by replicating the conditions used by Nowycky and Pinter (1993). Simulations usually required an integration time step of 1–4 μs.

Simulating the fluorescence changes

According to Grynkiewicz et al. (1985), the fluorescence, F, of a fluorescent indicator dye is given by

$$F = S_f[B^x] + S_b[CaB^x] = S_f([B^x_{total}] - [CaB^x]) + S_b[CaB^x] \Rightarrow F \propto \alpha[B^x_{total}] + (1 - \alpha)[CaB^x] \quad (9)$$

where S_f and S_b are the proportionality constants for the fluorescence of the free and Ca^{2+}-bound species of the indicator and $\alpha = S_f/S_b$. The proportionality constant drops out when the fractional fluorescence change (F_t/F_0) is calculated.

Blurring the simulated fluorescence changes

We cannot directly compare the fluorescence simulations with the experimental images because the observed fluorescence images were obtained with an epifluorescence microscope and are contaminated with out-of-focus information. The result is "blurred" images with reduced contrast and increased depth of field. On the other hand, the simulations provide a "nonblurred" ideal representation of the fluorescence gradients. Therefore, to allow a better comparison with experimental data we needed to mimic the blurring effect of the microscope. To this end, we constructed a three-dimensional model of the fluorescence simulations and "blurred" it, using the theoretical point spread function of the microscope, as previously described (Monck et al., 1992). Briefly, we used the simulated fluorescence data to construct a three-dimensional model of a 12.2-μm-diameter cell consisting of a stack of two-dimensional sections, 0.1 μm apart, assuming spherical symmetry. We then blurred this model, using the following algorithm:

$$O_j = \sum_{k=-m}^{m} I_{j+k} \cdot S_k \quad (10)$$

where O_j is the Fourier transform of the blurred image (simulation of the observed image), I_{j+k} is the Fourier transform of the successive sections above (positive k) and below (negative k) the in-focus image plane ($k = 0$), and S_k is the Fourier transform of the point spread function of the microscope for different degrees of defocus. The 12.2-μm-diameter model cell was divided into 125 sections ($m = 62$) of 0.1 μm each. Similar results were obtained with 25 sections ($m = 12$) of 0.5 μm or 63 sections ($m = 31$) of 0.2 μm each, indicating that the section spacing was not limiting.

Selection of parameters

For the selection of values for diffusion coefficients, affinities, and kinetic properties of exogenous Ca^{2+} buffers, we used the values generally used in previous studies (see Nowycky and Pinter, 1993; Klingauf and Neher, 1997). These are summarized in Table 1. Several values for the diffusion coefficient of BAPTA-derived Ca^{2+} indicators have been published: 50 $\mu m^2 \cdot s^{-1}$ for fura-2 in muscle (Timmerman and Ashley, 1986), 200 $\mu m^2 \cdot s^{-1}$ for fura-2 in patch-clamped chromaffin cells (Pusch and Neher, 1988), and 180 $\mu m^2 \cdot s^{-1}$ for fluo-3 in hair cells (Hall et al., 1997). Because none of the values were measured for rhod-2, we chose to use 200 $\mu m^2 \cdot s^{-1}$, as this was measured in adrenal chromaffin cells.

We have used the average measured Ca^{2+} current of 210 pA (207.8 ± 14.7 pA) for the simulations, and, as we are using a radial shell model, we implicitly assume an even distribution of Ca^{2+} channels. Although our pulsed laser imaging experiments (Monck et al., 1994; this paper) show that there is some nonuniformity in the Ca^{2+} increase, which is often larger at certain "Ca^{2+} hotspots," a Ca^{2+} increase is usually observed at all locations around the cell periphery; this is particularly obvious after longer depolarizations (Neher and Augustine, 1992; Monck et al., 1994). The increases at the hotspots rarely exceed twice the average increase around the cell periphery, suggesting that Ca^{2+} channels are distributed throughout the plasma membrane, with some regions of slightly higher density. When we ran simulations using a Ca^{2+} current of 500 pA, the Ca^{2+} gradient kinetics were similar, although there were correspondingly larger increases in Ca^{2+} concentration. Because the number and distribution of these Ca^{2+} hotspots are extremely variable between cells, we chose to use the average Ca^{2+} current instead of trying to estimate the Ca^{2+} current at the Ca^{2+} hotspots.

A major difficulty for the studies that used mathematical models to simulate Ca^{2+} gradients (Smith and Zucker, 1980; Connor and Nikolakapoulou, 1982; Zucker and Stockbridge, 1983; Chad and Eckert, 1984; Simon and Llinás, 1985; Neher, 1986; Sala and Hernández-Cruz, 1990; Nowycky and Pinter, 1993) was the choice of parameter values for the

TABLE 1 Parameters used in simulations with the radial diffusion model

Symbol	Definition	Value	Comment
Spatial parameters			
r	Cell radius	6.1 μm	Measured value. Average diameter was 12.2 ± 0.3 μm
δ	Shell thickness	0.1 μm	
Calcium parameters			
$[Ca^{2+}]_0$	Resting Ca^{2+} concentration	100 nM	
I_{Ca}	Whole cell current	210 pA	Measured value. Average was 207 ± 15 pA
τ	Time constant for Ca^{2+} current activation	3 ms	Measured value
D_{Ca}	Diffusion coefficient for Ca^{2+} in cytosol	200 $\mu m^2 \cdot s^{-1}$	Allbritton et al. (1992)
Ca^{2+}-ATPase			
K_m	Michaelis-Menten constant	0.83 μM	Sala and Hernández-Cruz (1990)
V_{max}	Maximum transport velocity	2 pmol $cm^{-2} \cdot s^{-1}$	
Exogenous buffers and indicator dyes			
EGTA	Total concentration	300 μM	In pipette solution
k_d	Dissociation constant	150 nM	Neher (1986)
k_{on}	Association rate constant	10 $mM^{-1}ms^{-1}$	Neher (1986)
k_{off}	Dissociation rate constant	0.0015 ms^{-1}	Neher (1986)
D_{EGTA}	Diffusion coefficient	200 $\mu m^2 \cdot s^{-1}$	Kushmerick and Podolsky (1969)
Rhod-2	Total concentration	200 μM	In pipette solution
k_d	Dissociation constant	1.88 μM	Escobar et al. (1997)
k_{on}	Association rate constant	69 $mM^{-1}ms^{-1}$	Escobar et al. (1997)
k_{off}	Dissociation rate constant	0.130 ms^{-1}	Escobar et al. (1997)
D_{rhod2}	Diffusion coefficient	200 $\mu m^2 \cdot s^{-1}$	As fura-2; Pusch and Neher (1988)
α	F_{min}/F_{max}	0.013	In vitro measurement
OG-BAPTA-5N	Total concentration	300 μM	In pipette solution
k_d	Dissociation constant	28 μM	DiGregorio et al. (1999)
k_{on}	Association rate constant	170 $mM^{-1}ms^{-1}$	DiGregorio et al. (1999)
k_{off}	Dissociation rate constant	4.8 ms^{-1}	DiGregorio et al. (1999)
D_{OGB-5N}	Diffusion coefficient	200 $\mu m^2 \cdot s^{-1}$	As fura-2; Pusch and Neher (1988)
α	F_{min}/F_{max}	0.04	In vitro measurement

properties of the endogenous Ca^{2+} buffers. An important part of this paper is to determine suitable values for these parameters by comparing simulated Ca^{2+} gradients with the measured Ca^{2+} gradients. In the course of this study, we have tested a large number of different values for the concentrations, affinities, and kinetic constants for endogenous buffers, based on the literature and on the experimental data described in this paper. Some of these values are summarized in Table 2 and will be discussed in detail throughout the Results and Discussion. (A more comprehensive collection of simulations of Ca^{2+} gradients is available from a WWW Supplement located at http://www.medsch.ucla.edu/som/physio/faculty/jrm/mss/BJSuppl.htm.)

Effect of ATP as a Ca^{2+} buffer

We investigated the effect of ATP as a Ca^{2+} buffer, using the parameters given by Klingauf and Neher (1997). ATP at 2 mM, the concentration in the pipette solution, had negligible effects on the magnitude and kinetics of the Ca^{2+} concentration and Ca^{2+}-indicator complex concentration or on the fractional fluorescence change in simulations with mobile Ca^{2+} buffers (unpublished data; see the WWW Supplement). For example, ATP decreased the peak fractional fluorescence change at the end of the depolarization by less than 4% (1.60 to 1.58) in the outer shell; the decrease was much smaller in other shells. Because we observed no effects on the kinetics of Ca^{2+} gradient development or dissipation, we have ignored ATP in simulations of the experimental conditions. However, we included ATP in the simulations of the Ca^{2+} gradients in the absence of exogenous mobile Ca^{2+} buffers (Fig. 9), where the effect of ATP is significant, as it is the only mobile Ca^{2+} buffer.

Analysis of gradient dissipation

To compare the dissipation of the Ca^{2+} gradient in experiments and simulations, we defined the difference between the fluorescence signal at the cell periphery and the center of the cell, $(F_t/F_o)_{edge} - (F_t/F_o)_{center}$, as a parameter to represent the size of the Ca^{2+} gradient at a particular time. The decay of $(F_t/F_o)_{edge} - (F_t/F_o)_{center}$ after the depolarization was well represented by the sum of two exponentials, $A_1 \cdot e^{-t/\tau 1} + A_2 \cdot e^{-t/\tau 2}$, one with a fast time constant (τ_1) (typically 4–10 ms) and the other with a slow time constant (τ_2), which was strongly dependent on the type and amount of fixed buffer. This relationship applied to the measured fluorescence gradients and all of the simulations studied in which a significant amount of immobile endogenous buffer was included. When no fixed buffer was added to the model (Table 2, simulation a), only one exponential ($\tau = 7.9$ ms) was necessary to fit the curve. We observed that this fast time constant is strongly influenced by the diffusion coefficient of the mobile exogenous buffers (see Table 2, simulations q–t). On the other hand, we found τ_2 to be a useful parameter for quantifying the dissipation time of the Ca^{2+} gradients. The dissipation of the gradient after a few tens of milliseconds is dominated by the slower exponential, because the magnitude of the faster component has become very small. We found that τ_2 increases linearly with the buffer capacity of immobile buffers over the range 100-1500 when the dissociation rate constant, k_{off}, is greater than 0.01 ms^{-1} (unpublished data; see the WWW Supplement). Because the dissipation time is calculated from relative fluorescence changes (F_t/F_o), which are approximately linear for low indicator saturations, this relationship between dissipation time (τ_2) and buffer capacity is relatively insensitive to the absolute Ca^{2+} concentration estimates. The dissipation time constant (τ_2) changes by less than 15% with twofold errors in the absolute Ca^{2+} concentration estimate.

TABLE 2 Properties of Ca^{2+} gradients simulated using endogenous buffers with different parameters

	Properties of endogenous buffer					Diffusion coefficient‡	Properties of fluorescence gradient dissipation			Fluorescence (F_t/F_0) after 40-ms depolarization	
	Concentration (mM)	K_d (μM)	k_{on} ($mM^{-1} \cdot ms^{-1}$)	k_{off} (ms^{-1})	κ	D ($\mu m^2 \cdot s^{-1}$)	τ_1 (ms^{-1})	τ_2 (ms^{-1})	A_2 (%)	Edge (shell 0)	Center (shell 60)
Exp.*	—	—	—	—	—	—	7.6	155.9	60	1.87	1.26
a	0	—	—	—	0	200	7.9	—	—	3.64	2.60
b	4	100	100	10	40	200	13.5	—	—	3.09	2.10
c	0.121	1	50	0.05	100	200	5.2	27.5	47	2.93	2.01
d	0.605	1	50	0.05	500	200	4.9	74.1	58	1.97	1.40
e	0.847	1	50	0.05	700	200	5.0	95.8	60	1.78	1.31
f	1.21	1	50	0.05	1000	200	5.1	128.7	62	1.60	1.23
g	1.815	1	50	0.05	1500	200	5.2	183.7	65	1.43	1.15
h	100.2	100	0.5	0.05	1000	200	4.1	152.6	66	1.52	1.20
i	10.2	10	5	0.05	1000	200	4.1	149.8	65	1.53	1.20
j	0.4	0.1	500	0.05	1000	200	7.2	91.9	43	1.95	1.34
k	0.6	0.1	500	0.05	1500	200	8.4	136.5	41	1.74	1.25
l	1.21	1	1	0.001	1000	200	7.4	—	—	3.17	2.26
m	1.21	1	5	0.005	1000	200	6.0	271.0	9	2.36	1.69
n	1.21	1	10	0.01	1000	200	5.3	200.3	20	2.01	1.47
o	1.21	1	25	0.025	1000	200	4.7	147.8	44	1.72	1.29
p	1.21	1	100	0.1	1000	200	8.8	124.9	73	1.54	1.19
q	1.815	1	50	0.05	1500	500	2.7	137.2	60	1.34	1.19
r	0.968	1	50	0.05	800	100	7.3	146.5	61	1.85	1.23
s	0.605	1	50	0.05	500	50	9.0	144.9	59	2.38	1.29
t	0.121	1	50	0.05	100	10	18.7	154.1	51	4.38	1.51

*Values obtained from the experiments shown in Fig. 3, *B* and *C,* for comparison.
‡Diffusion coefficient used for mobile species (EGTA, Ca^{2+}, rhod-2 or OGB-5N).

It is also worth noting that when gradients were simulated with low fixed buffer capacities (Table 2, simulation b), the gradient dissipated with a single exponential.

Statistical analysis

Statistical analysis and curve fitting used the built-in functions of Origin 5.0 (Microcal Software, Northampton, MA). To fit the time constants of the Ca^{2+} gradient dissipation times, we used the nonlinear curve-fitting option, which uses a Levenberg-Marquardt algorithm. To determine whether the Ca^{2+} gradients were maintained at longer times (>200 ms) after the pulse, when the gradients have become very shallow, we used a linear regression analysis of the F_t/F_o half-profiles (n represents the number of pixels in the half-profile). In the test, we indicate the goodness of fit with the correlation coefficient r and the probability that the slope is different from zero (p_{slope}). This probability was obtained using a t value (parameter estimate/standard error) for testing whether the slope is different from zero.

RESULTS

Measurement of Ca^{2+} gradients evoked by depolarizing stimuli

Temporal resolution is conventionally obtained by triggering an event and taking measurements as rapidly as possible thereafter. For imaging experiments this approach is severely limited by the speed of the imaging hardware, and temporal resolution is attained at the expense of spatial resolution. An alternative approach is to take a single "snapshot" image from a series of successive events, with each measurement delayed differently with respect to the event trigger. With this approach, images of a specimen are captured while the whole image field is briefly illuminated with a pulsed laser (Kinosita et al., 1988; Monck et al., 1994). Because the illumination period is limited (<1 μs), the image is a "snapshot" of the event at the time of the laser pulse and is not limited by the speed of the imaging device (a cooled CCD camera). Because of the high-intensity laser illumination, we were able to obtain images with high spatial resolution and a good signal-to-noise ratio. As long as the response can be reproduced consistently, as accomplished in excitable cells, very high time resolutions can be obtained. In fact, for the experiments described in this paper, the temporal limitation is the binding kinetics of the Ca^{2+} indicator. Finally, because each image required a different stimulus, small variations in the Ca^{2+} measurements may occur because of the slight Ca^{2+} current rundown and/or variation in the cellular Ca^{2+} handling.

Development of Ca^{2+} gradients during depolarizing stimuli

Fig. 1 *A* shows the development of the Ca^{2+} gradient during a 40-ms depolarization in a cell loaded with the Ca^{2+} indicator rhod-2. The color images are pseudocolor F_t/F_o ratio images representing fluorescence changes captured at

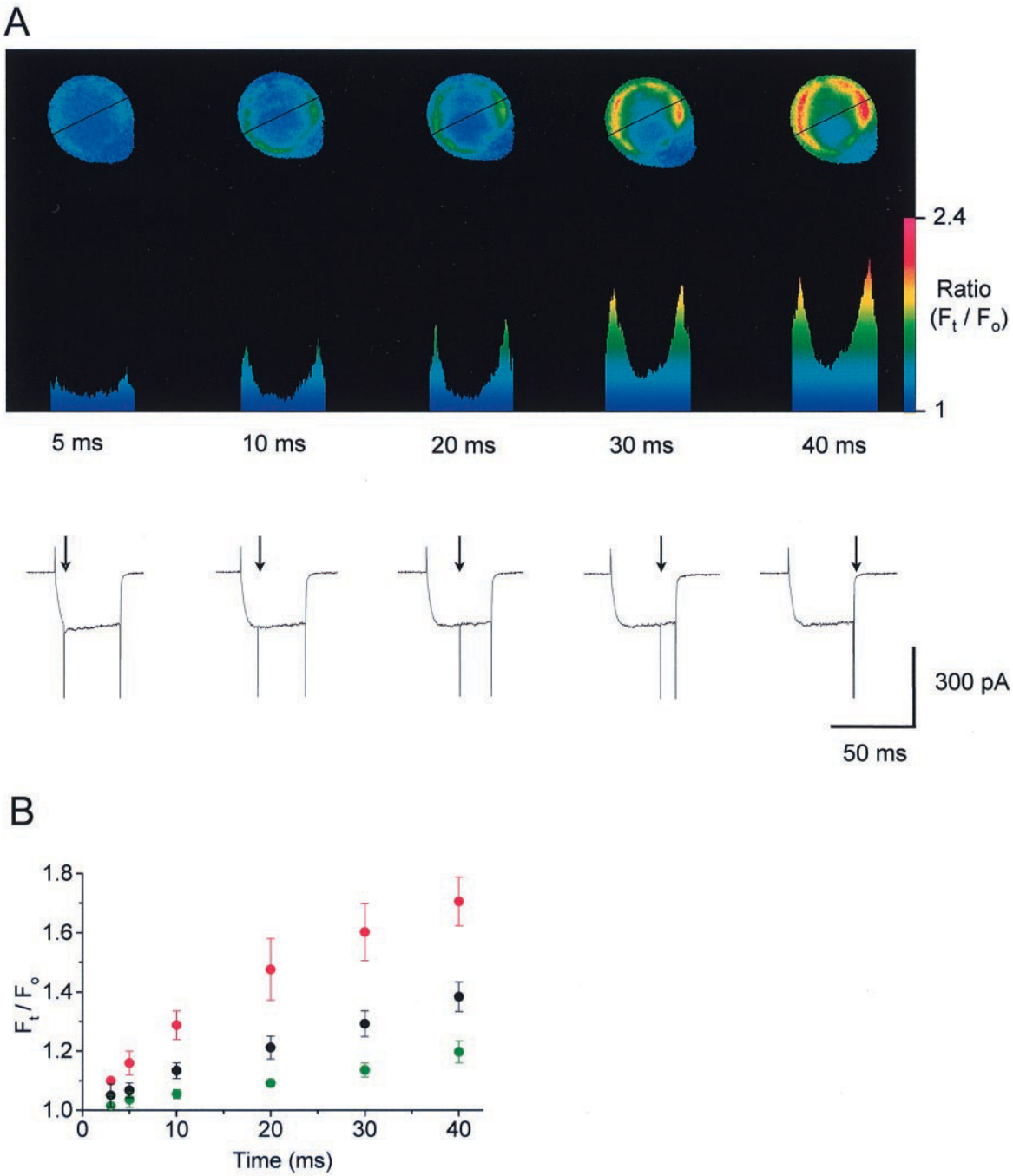

FIGURE 1 Time course of the development of Ca^{2+} gradients measured using pulsed laser imaging of rhod-2 loaded cells. Ca^{2+} gradients were induced by a 40-ms depolarization in patch-clamped adrenal chromaffin cells. (*A*) Sequence of pseudocolor F_t/F_o ratio images representing fluorescence changes captured at different times after the start of the depolarization (see Materials and Methods). Below each image is the profile of the F_t/F_o values for a section along the line marked in the image. The Ca^{2+} currents associated with each Ca^{2+} measurement are shown below the corresponding images. The arrows mark the time of the transient laser illumination for each measurement, which is often associated with a current artifact. (*B*) Summary of data from five measurements in different cells, showing the mean ± SE at the edge of the cell (*red circles*), the center of the cell (*green circles*), and the spatially averaged values from the entire cell (*black circles*).

defined times after the start of the depolarization (see Materials and Methods). Each image is taken with a different delay with respect to the beginning of the depolarization. Below each image is a profile for a section through the center of the cell. These data show that a submembrane Ca^{2+} gradient can be recorded at early times (<10 ms). At later times the size of the increase beneath the membrane becomes larger, and an increase in F_t/F_o at the center of the

cell is also observed. Fig. 1 *B* shows data averaged from several cells and compares the changes in F_t/F_o at the edge of the cell with the changes in F_t/F_o at the center of the cell and the spatially averaged values. The increase in F_t/F_o at the center of the cell becomes significant at 10 ms ($p < 0.05$, $n = 5$ cells) and continues to increase until the end of the depolarizing stimulus.

Fig. 2 shows an analysis of the Ca^{2+} gradient profiles. The profiles of the Ca^{2+} gradients captured 10, 20, 30, and 40 ms after the start of the depolarizing pulse are shown for several cells (Fig. 2, *A–D*). Although there are small differences between the cells, the changes follow a similar pattern, which is well represented by the averages (Fig. 2 *E*).

Dissipation of Ca^{2+} gradients after depolarizing stimuli

Fig. 3 *A* shows the dissipation of the Ca^{2+} gradient after a 40-ms pulse. The images shown are from the cell used to show the development of the Ca^{2+} gradient in Fig. 1 *A*. These images and the profiles show that Ca^{2+} gradients are maintained for several hundred milliseconds. Data averaged from several cells (Fig. 3 *B*) confirm this slow pattern of Ca^{2+} gradient dissipation. Note that we use gradient dissipation to describe the time period over which the Ca^{2+} concentration in the cell becomes homogeneous. After the gradient is completely dissipated the Ca^{2+} concentration is still elevated and decays more slowly to resting levels. Fig. 3 *C* shows the time course of gradient dissipation, calculated as the difference between F_t/F_o at the edge of the cell and at the center, as described in Materials and Methods. The data were normalized to the value at the end of the depolarization in individual experiments. The gradient dissipation was fitted with two exponentials, representing a fast decay that occurs in tens of milliseconds ($\tau_1 = 7.6 \pm 2.9$ ms) and a slower decay with a time constant, τ_2, of 155.9 ± 40.9 ms. The 95% confidence limits for the fit of the slow dissipation time constant gave a range of 114–218 ms.

Fig. 4 shows an analysis of the profiles of the Ca^{2+} gradients during dissipation. The half-profiles at the end of a 40-ms depolarizing pulse (Fig. 4 *A*) and the half profiles 160 ms, 360 ms, and 460 ms later (Fig. 4, *B–D*) are shown

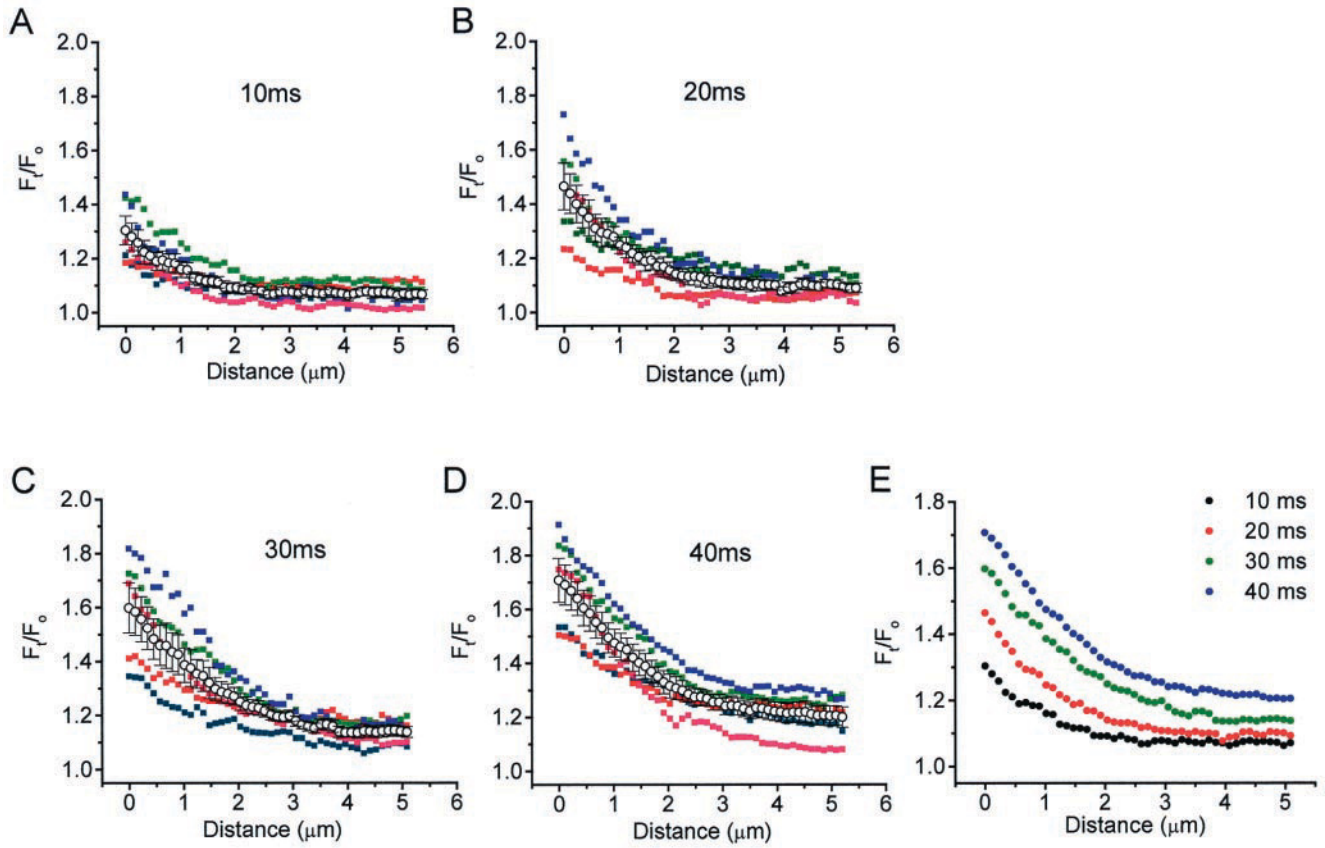

FIGURE 2 Profile analysis of developing Ca^{2+} gradients during depolarization. Spatial analysis of the Ca^{2+} gradients in several cells from experiments similar to the one shown in Fig. 1. (*A*) Comparison of F_t/F_o half-profiles from several cells representing Ca^{2+} gradients captured 10 ms after the start of the depolarizing pulse. (*B–D*) Similar comparisons representing Ca^{2+} gradients captured after 20, 30, and 40 ms. It is clear that, although there are small differences between the cells, the pattern of the change is similar and is well represented by the averages. (*E*) Half-profiles showing the average F_t/F_o changes from several cells at 10, 20, 30, and 40 ms after the start of the depolarizing pulse.

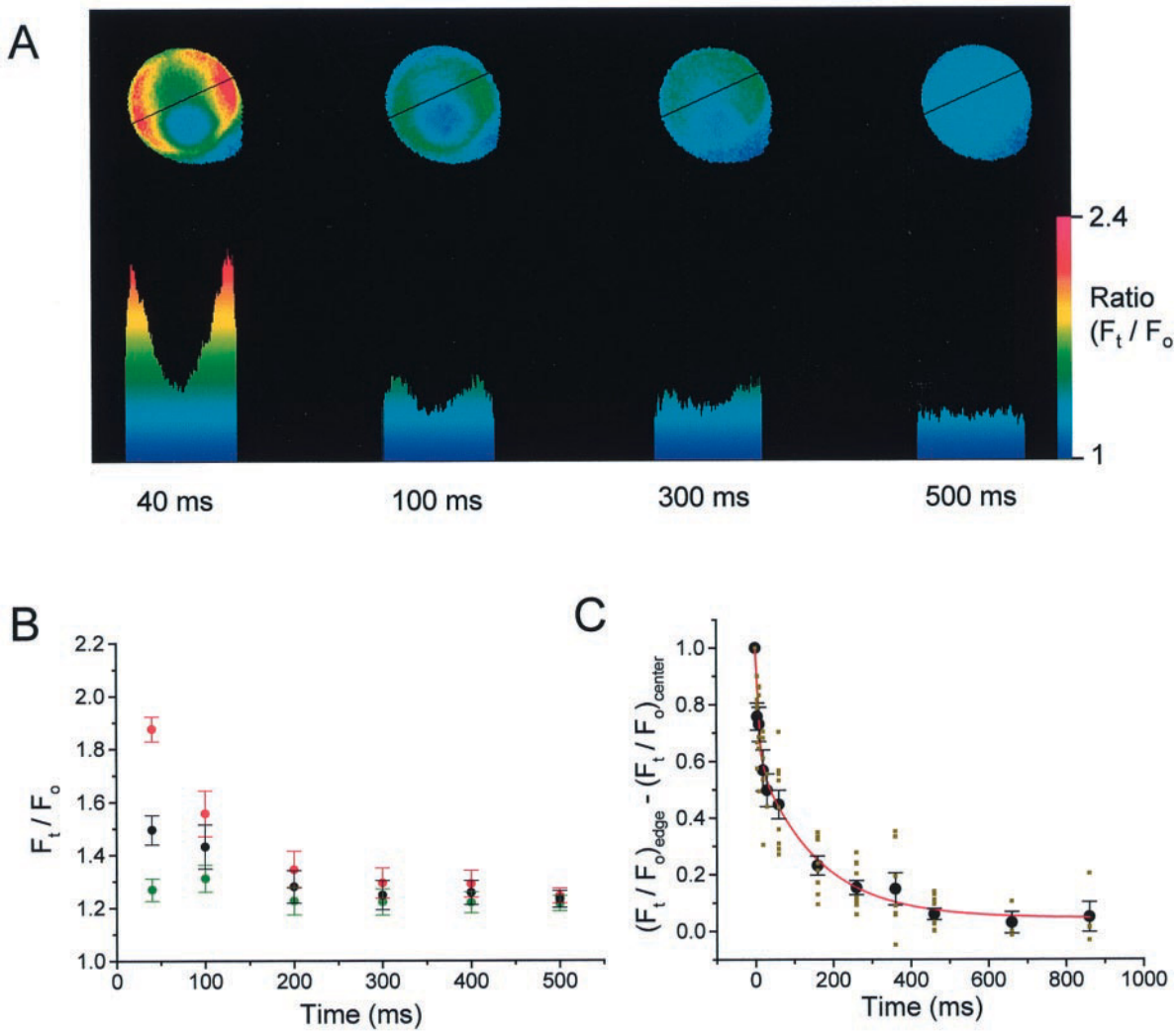

FIGURE 3 Ca^{2+} gradient dissipation after short depolarizing pulses. Time course of Ca^{2+} gradient dissipation after a 40-ms depolarization in rhod-2-loaded chromaffin cells. (*A*) Sequence of F_t/F_o ratio images showing the time course of Ca^{2+} gradient dissipation. The indicated times refer to the time from the beginning of the depolarizing pulse. Below each image is the profile showing the F_t/F_o ratio values along the lines shown in the images. (*B*) Summarized values from measurements on different cells ($n = 8$), showing the mean ± SE at the edge of the cell (*red circles*), the center of the cell (*green circles*), and the spatially averaged F_t/F_o values from the entire cell (*black circles*). (*C*) The time course of the dissipation of the Ca^{2+} gradient, calculated as the difference between F_t/F_o at the edge of the cell and at the center, which has been normalized to the value at the end of the depolarizing pulse in each cell. The decay of the gradient is well represented by the sum of two exponentials (*red line*) with time constants $\tau_1 = 7.6 \pm 2.9$ ms and $\tau_2 = 155.9 \pm 40.9$ ms and magnitudes 0.38 ± 0.07 and 0.58 ± 0.06, respectively. The individual experimental values that were used to fit the curve are shown as small green squares. The averaged values are shown as black circles with standard error bars.

for several individual cells. Fig. 4 *E* summarizes the average half-profiles at different times during the dissipation of the Ca^{2+} gradient. These data show that the Ca^{2+} at the edge starts to decrease after the end of the depolarization, but further inside the cell the Ca^{2+} concentration continues to increase for at least 60 ms, as Ca^{2+} and the Ca^{2+}-indicator complex diffuse toward the cell center. Between 160 and 460 ms after the end of the depolarizing pulse the gradients became progressively smaller and shallower, but could still be resolved. Analysis of the half-profiles obtained at 360 ms shows that the gradients were significant in six of six cells ($p_{slope} > 0.99$), whereas after 460 ms the gradients were significant in five of seven cells ($p_{slope} > 0.99$ (four cells), $p_{slope} > 0.97$ (one cell)). However, the average gradient calculated from the seven cells was still significant after 460 ms ($p_{slope} > 0.99$). Finally, the gradients became insignificant at later times (e.g., after 660 ms, $p_{slope} < 0.25$).

Role of cellular Ca^{2+} transport in determining Ca^{2+} gradient properties

Estimation of the total amount of Ca^{2+} entering from the Ca^{2+} current integral shows that most of the Ca^{2+} is not

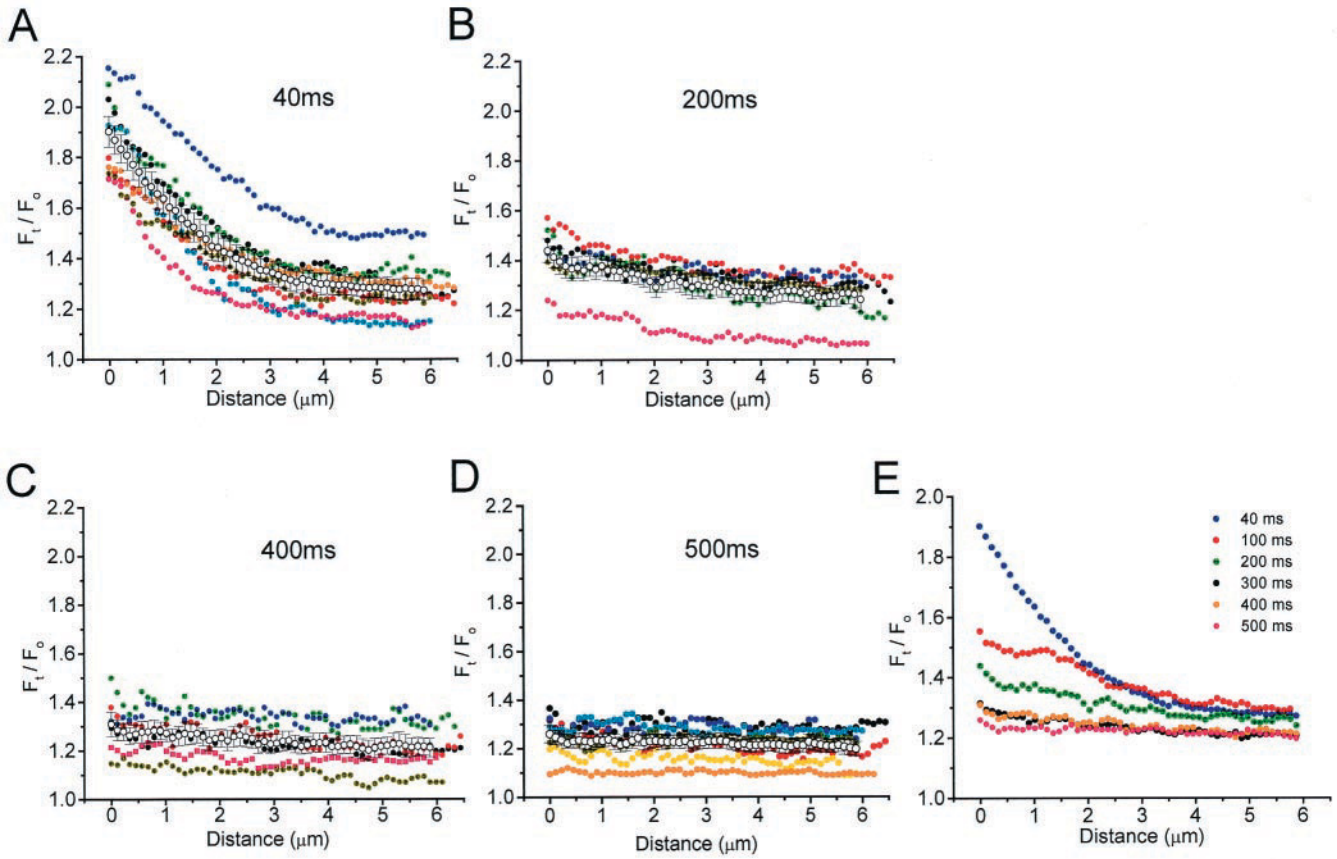

FIGURE 4 Profile analysis of dissipating Ca^{2+} gradients after depolarization. Spatial analysis of the Ca^{2+} gradients in several cells from experiments similar to the one shown in Fig. 3. (*A*) Comparison of F_t/F_o half-profiles from several cells representing Ca^{2+} gradients captured at the end of a 40-ms depolarizing pulse. (*B–D*) Half-profiles from several cells 160 ms, 360 ms, and 460 ms after the end of the pulse. (*E*) The averages at different times during the dissipation of the Ca^{2+} gradient. It is clear that during the first 60 ms after the pulse there is a decrease at the edge of the cell and an increase at the center of the cell as the Ca^{2+} ions diffuse to the center of the cell, although there is still a prominent Ca^{2+} gradient. The fluorescence gradients at 160, 260, 360, and 460 ms after the end of the depolarizing stimulus become progressively smaller and shallower but are still significant.

available in the free ionized form. We calculate that during a 40-ms depolarization 4×10^{-17} moles of Ca^{2+} enter the cell, for an average Ca^{2+} current of 207.8 ± 14.7 pA. This is equivalent to 46 μM, based on the average diameter of the cells used in the experiments (12.2 ± 0.3 μm). From the spatially averaged fluorescence change (F_t/F_o = 1.44 ± 0.06), we estimate that the average Ca^{2+} change at the end of a 40-ms pulse is 59 ± 9 nM. Therefore, only ~0.1% of the Ca^{2+} entering the cell is in the free ionized form in the cytosol. Most of the Ca^{2+} must be bound to cytosolic Ca^{2+} buffers or removed from the cytosol by Ca^{2+} transport mechanisms.

We used a pharmacological approach to assess the possible contribution of active Ca^{2+} uptake by intracellular stores such as endoplasmic reticulum and mitochondria to cellular buffering. Fig. 5, *A, B*, and *E*, shows that thapsigargin, an inhibitor of SERCA Ca^{2+}-ATPases that prevents Ca^{2+} uptake into endoplasmic reticulum, had no effect on the size of the Ca^{2+} gradients or their dissipation (compare with Figs. 3 and 4). In these experiments, 1 μM thapsigargin was added to both the extracellular solution and the pipette solution at least 10 min before data recording. The sizes of the gradients during development were also unchanged in the presence of thapsigargin (unpublished data). Note that the density of the Ca^{2+} current (current divided by cell membrane capacitance) was not significantly different in the thapsigargin experiments (61.7 ± 8.3 pA/pF), compared with the controls (57.14 ± 6.42 pA/pF). Fig. 5 *B* shows that there is still a shallow gradient 460 ms after the end of the pulse. Linear regressions performed on the half-profiles demonstrated significant slopes in five of six cells after 460 ms ($p_{slope} > 0.998$). We also estimated that, in the presence of thapsigargin, the Ca^{2+} gradient dissipated with a time constant (τ_2) of 169.5 ± 30.6 ms (Fig. 5 *E*), similar to the 155.9 ± 40.9 ms for controls (Fig. 5 *E*, *dotted line*). Finally, thapsigargin did not significantly modify the decay of the average Ca^{2+} after the end of the depolarization (compare Figs. 3 *B* and 5 *A*), suggesting that Ca^{2+} uptake by the

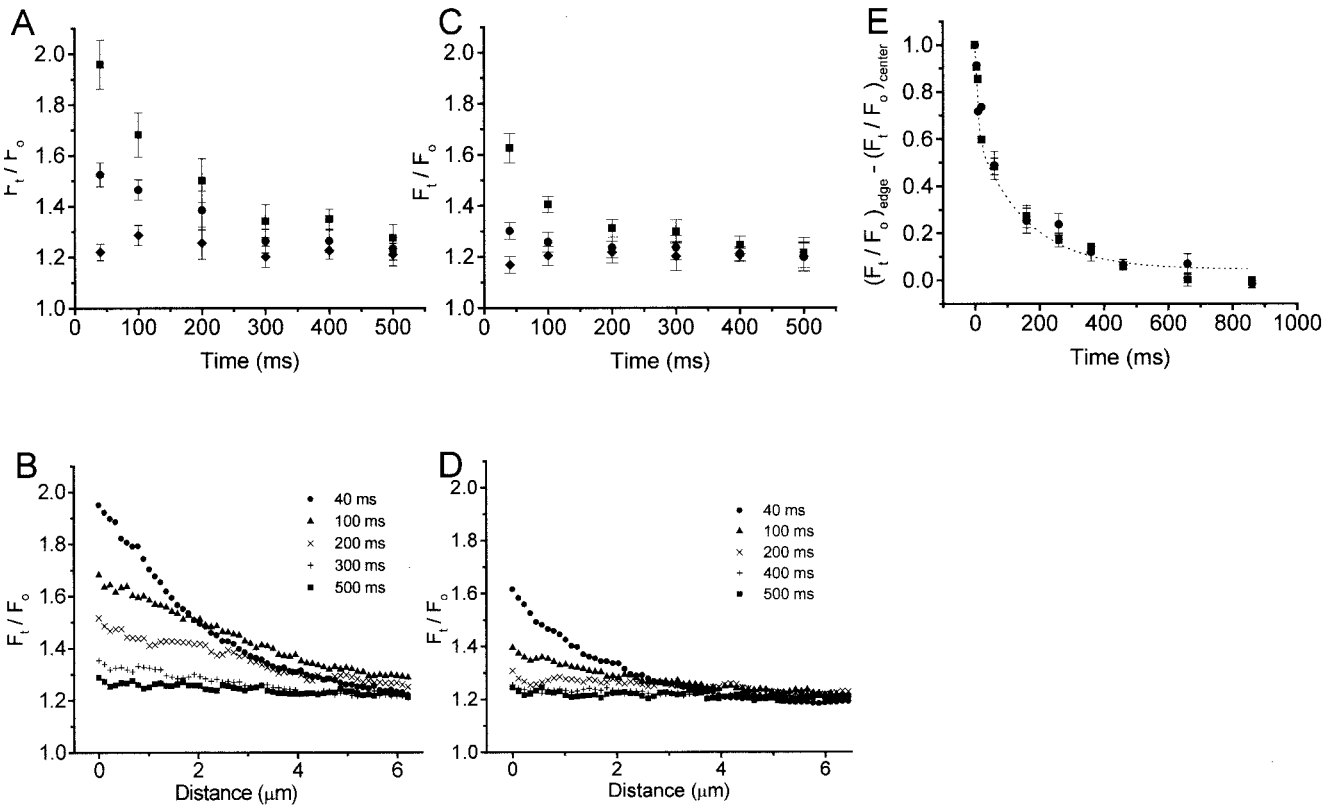

FIGURE 5 Effect of inhibiting intracellular Ca^{2+} stores on Ca^{2+} gradient dissipation. (A) Time course of Ca^{2+} gradient dissipation after 40-ms depolarizing pulses in rhod-2-loaded chromaffin cells in the presence of 1 μM thapsigargin. (B) F_t/F_o half-profiles, averaged from six cells at different times during dissipation of the Ca^{2+} gradient in the presence of thapsigargin. (*C*) Time course of Ca^{2+} gradient dissipation in the presence of 1 μM FCCP plus 0.2 μM oligomycin. (*D*) F_t/F_o half-profiles, averaged from seven cells in the presence of FCCP and oligomycin. (*E*) Time courses of the dissipation of the fluorescence gradient, calculated as the difference in F_t/F_o between the edge and center of the cell and normalized to the change at the end of the depolarizing pulse. The data are for experiments in the presence of thapsigargin (■) or FCCP + oligomycin (●). The dotted line, which shows the double-exponential fit to the control data (Fig. 3 *C*), illustrates the lack of effect of both pharmacological treatments on Ca^{2+} gradient dissipation (τ_2 = 169.5 ± 30.6 and 180.6 ± 44.2 ms for thapsigargin and FCCP + oligomycin, respectively).

endoplasmic reticulum does not play a significant role in lowering cytosolic Ca^{2+}, at least on the time scale of our experiments.

To inhibit Ca^{2+} uptake by mitochondria, we used a combination of carbonylcyanide *p*-trifluoro-methoxyphenylhydrazone (FCCP), a mitochondrial uncoupler, and oligomycin, an inhibitor of the mitochondrial H^+-ATPase. We used oligomycin, in addition to FCCP, to prevent rapid ATP hydrolysis by the H^+-ATPase in uncoupled mitochondria, as this could cause local depletion of ATP and reduce uptake by other intracellular stores. FCCP (1 μM) and oligomycin (0.2 μM) were added to the pipette solution and the extracellular solution. Under these experimental conditions the fluorescence changes were slightly smaller than those of the controls. At the end of the depolarization the F_t/F_o signal at the edge of the cell and the spatially averaged value were 1.62 ± 0.06 and 1.30 ± 0.03, respectively, compared to 1.81 ± 0.05 and 1.50 ± 0.06 for the control experiments. The smaller values are probably due to a decrease in Ca^{2+} current density, which was reduced from 57.14 ± 6.42 pA/pF (controls) to 41.26 ± 8.73 pA/pF (FCCP + oligomycin). As under control conditions, Ca^{2+} gradients were maintained for hundreds of milliseconds. The Ca^{2+} gradients were still significant in all cells 360 ms after the end of the pulse (5/5, $P_{slope} > 0.99$) and in three of four cells after 460 ms ($P_{slope} > 0.99$). A comparison of the time course of Ca^{2+} gradient dissipation in the presence and absence of mitochondrial inhibitors clearly shows that inhibiting mitochondrial Ca^{2+} uptake did not change the dissipation of the Ca^{2+} gradients (Fig. 5 *E*). The dissipation time constant (τ_2) was 180.6 ± 44.2 ms in the presence of mitochondrial inhibitors. Note, however, that the average Ca^{2+} decays more slowly in the presence of FCCP than in control conditions (compare Figs. 3 *B* and 5 *C*). The average fluorescence value decreases from 1.30 ± 0.03 at the end of the depolarizing pulse (40 ms) to 1.20 ± 0.05 (n = 7 cells) after 500 ms in the presence of mitochondrial inhibitors, compared with a decrease from 1.50 ± 0.06 to 1.23 ± 0.03 (n = 9 cells) in controls (a decrease of 0.10 compared with 0.27) or a decrease from 1.53 ± 0.05 to 1.23 ± 0.04 (n =

6 cells) with thapsigargin. This effect is consistent with the presence of some Ca^{2+} uptake by mitochondria under our control conditions (see also Herrington et al., 1996). Alternatively, the reduced Ca^{2+} clearance may result from the smaller Ca^{2+} elevation that occurs in the presence of mitochondrial inhibitors.

A number of studies have reported a role of the Na/Ca exchange in cytosolic Ca^{2+} clearance after stimulation (Herrington et al., 1996; Pan and Kao, 1997; Tang et al., 2000). Although the effects of the Na/Ca exchanger were generally seen on time scales (5–20 s) longer than those in our experiments, we nonetheless considered the contribution of the Na/Ca exchanger to the dissipation of the Ca^{2+} gradients. To address this issue, we replaced Na^+ with *N*-methyl-D-glutamine, in both the extracellular and pipette solutions. We found that the Ca^{2+} increase at the end of a 40-ms depolarization was not increased in the absence of extracellular Na^+. The F_t/F_o value at the edge of the cell was 1.65 ± 0.07 (three cells), which is slightly smaller than the control value. This reduction is probably due to the reduced size of the Ca^{2+} currents under zero Na^+ conditions (158 ± 36 pA versus 208 ± 15 pA in controls), an effect of Na^+ replacement that was previously described by Pan and Kao (1997). Thus our data indicate that Na/Ca exchange does not significantly change the Ca^{2+} response during a short depolarizing stimulus and is therefore consistent with previous reports (Herrington et al., 1996; Pan and Kao, 1997). More importantly, persistence of the Ca^{2+} gradients was not reduced under zero Na^+ conditions. The fluorescence gradient decayed with a time constant (τ_2) of 183 ± 28 ms (three cells). Therefore, we conclude that the Na/Ca exchanger does not participate in Ca^{2+} gradient dissipation. This result does not preclude a role for the Na/Ca exchanger in cytosolic Ca^{2+} clearance after Ca^{2+} gradient dissipation, as observed by others (Herrington et al., 1996; Pan and Kao, 1997; Tang et al., 2000).

The results in this section indicate that none of the major cellular Ca^{2+} transport mechanisms that are involved in cytosolic Ca^{2+} clearance after stimulation affect the dissipation of the Ca^{2+} gradient within the 500-ms period after a depolarization. Because mitochondrial and endoplasmic reticular Ca^{2+} stores do not appear to behave like an active Ca^{2+} buffering system that might slow Ca^{2+} gradient dissipation, we conclude that the Ca^{2+} redistributions during Ca^{2+} gradient dissipation are primarily due to diffusion and binding to passive Ca^{2+} buffers.

Effects of immobile endogenous buffers

We used a radial diffusion model to simulate the Ca^{2+} gradients that would be generated in the presence of various endogenous Ca^{2+} buffers. Our calculation of the fraction of Ca^{2+} that remains free after entering the cell (previous section) suggested that the cytosolic buffers must bind on the order of 99.9% of the Ca^{2+} ion entering the cell. Calculation of the buffer capacity, the ratio of the concentration of Ca^{2+} bound to buffers over the free Ca^{2+} concentration (Neher and Augustine, 1992), requires an estimate of the accessible cytosolic volume, i.e., the volume of the cytoplasm minus the volume occupied by chromaffin granules, endoplasmic reticulum, and other organelles. We do not know the accessible volume in adrenal chromaffin cells, but for values ranging from 40% to 80% the total buffer capacities may be estimated as 975-1950. Because the buffer capacity of the mobile Ca^{2+} buffers in the pipette solution (EGTA and rhod-2) is 816 (calculated at 100 nM resting Ca^{2+}), the endogenous buffer capacity would be in the range of 160-1130. Clearly, the buffer capacity estimated in this way is very dependent on the accessible volume assumed and is very unsatisfactory. Thus we first considered the effect of varying the buffer capacity on the pattern of Ca^{2+} gradient development and dissipation. As the Ca^{2+} gradient dissipation is relatively slow, we made the initial assumption that endogenous buffers are likely to be immobile or poorly mobile. In contrast, a mobile buffer would cause faster gradient dissipation by binding Ca^{2+} and diffusing to the cell center as the Ca^{2+}-bound complex.

Fig. 6 shows some examples of simulations generated using the radial diffusion model, where various concentrations of immobile Ca^{2+} buffers were included to try to reproduce the sizes of the fluorescence changes and the dissipation times of the measured Ca^{2+} gradients. We used a buffer with a k_{off} of 0.05 ms^{-1} and a k_{on} of 50 $mM^{-1} \cdot ms^{-1}$, which gave a K_d of 1 μM. We chose this k_{off} value because it gave the best approximations of the relative sizes of the slow and fast exponential components for gradient dissipation, regardless of the K_d and buffer capacity used (see later for more details). The simulations obtained using buffer capacities of 100, 500, 1000, and 1500 are shown in Fig. 6, *A–D*. The dissipation time constants (τ_2) for these simulations were 28, 74, 129, and 184ms, respectively (Table 2). The simulation with the buffer capacity of 1000 gave the closest match to the measured dissipation time constant of 155.9 ± 40.9 ms but was still faster, suggesting that a slightly higher buffer capacity would be better. However, the size of the measured fluorescence changes was better matched when a slightly lower buffer capacity (e.g., 700) was used (Table 2, simulation e). Lower buffer capacities resulted in much faster dissipation times and larger Ca^{2+} changes (Fig. 6 *A*) than those measured (Figs. 3 and 4).

We next examined how the affinity of the endogenous Ca^{2+} buffer affected the simulations. Results from such simulations for K_d values of 0.1, 1 and 10 μM, each with a buffer capacity of 1000, are shown in Fig. 6. In this series of simulations, the K_d was adjusted by changing the k_{on} and keeping k_{off} constant at 0.05 ms^{-1}. A buffer with a K_d of 100 μM resulted in a simulation that was virtually superimposable on that for the buffer with the K_d of 10 μM (unpublished data; see simulation h in Table 2 and the

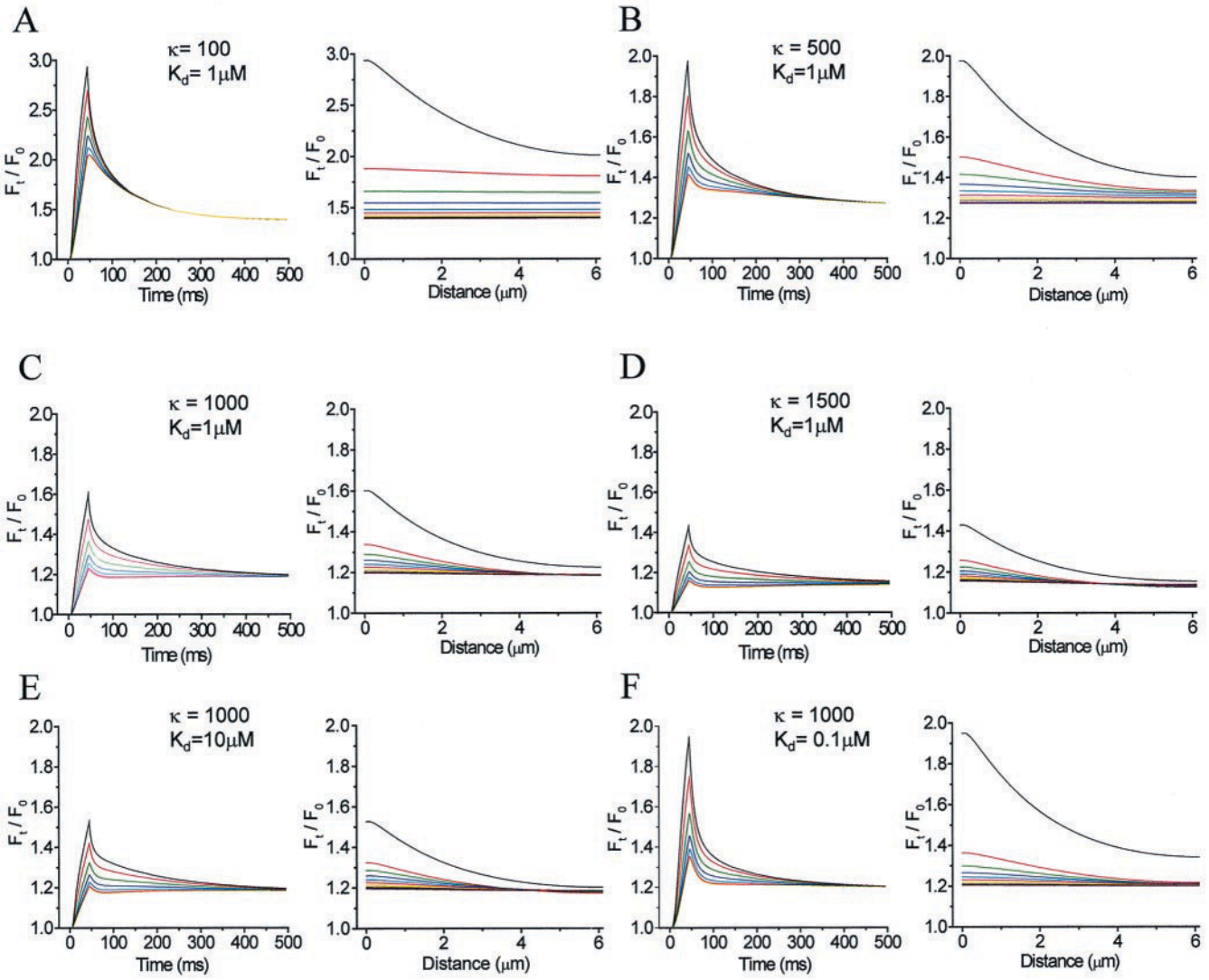

FIGURE 6 Simulation of Ca^{2+} gradients with immobile endogenous buffers with different buffer capacities and dissociation constants. Simulated changes in the rhod-2 fluorescence ratio in response to Ca^{2+} entry during a 40-ms depolarizing pulse. (*A–D*) Simulations performed in the presence of different amounts of an immobile endogenous Ca^{2+} buffer. The left panels show the time courses for the fluorescence changes that would be measured in shells 0, 10, 20, 30, 40, 50, and 60 corresponding to the immediate submembrane shell and the shells 1, 2, 3, 4, 5, and 6 μm from the cell membrane. The right panel shows the half-profiles of the fluorescence for a section through the center of the cell at the end of the depolarizing pulse (40 ms) and at 50-ms intervals thereafter. The properties of the endogenous buffer were K_d = 1 μM, k_{on} = 50 $mM^{-1}{\cdot}ms^{-1}$ and k_{off} = 0.05 ms^{-1}, at the following concentrations: 0.12 mM (κ = 100) (*A*), 0.61 mM (κ = 500) (B), 1.21 mM (κ = 1000) (*C*), 1.83 mM (κ = 1500) (*D*). (*E* and *F*) Simulated fluorescence ratio changes in the presence of an endogenous Ca^{2+} buffer with a buffer capacity of 1000 and with K_d values of 10 μM (*E*) and 0.1 μM (*F*), respectively (k_{off} = 0.05 ms^{-1}, and k_{on} was modified to change the K_d appropriately).

WWW Supplement). Dissipation times within the 95% confidence limits of the measured dissipation times (114–218 ms) were obtained for K_d values of 100 μM (not shown), 10 μM (Fig. 6 *E*), and 1 μM (Fig. 6 *C*). The gradients dissipated at a slightly slower rate for a 10 μM K_d buffer (τ_2 = 150 ms) than for a 1 μM K_d buffer (τ_2 = 129 ms) (Fig. 6 and Table 2), suggesting that a slightly lower buffer capacity is needed with lower affinity buffers. On the other hand, a higher affinity buffer needs to be present at higher buffer capacities. For example, a buffer with a K_d of 0.1 μM and a buffer capacity of 1000 (Fig. 6 *F*) gave a faster dissipation time (τ_2 = 92 ms), but a reasonable dissipation time can be obtained by increasing the buffer capacity to 1500 (Table 2, simulation k).

Finally, we examined the effects of changing the kinetics of the Ca^{2+} buffer. Fig. 7 shows four simulations with the same buffer capacity (κ = 1000) and K_d (1 μM), but different rate constants. With k_{off} ranging from 0.01 ms^{-1} to 0.1ms^{-1}, slower rate constants tended to increase the dissipation time, τ_2 (Table 2). Thus the gradients dissipate more

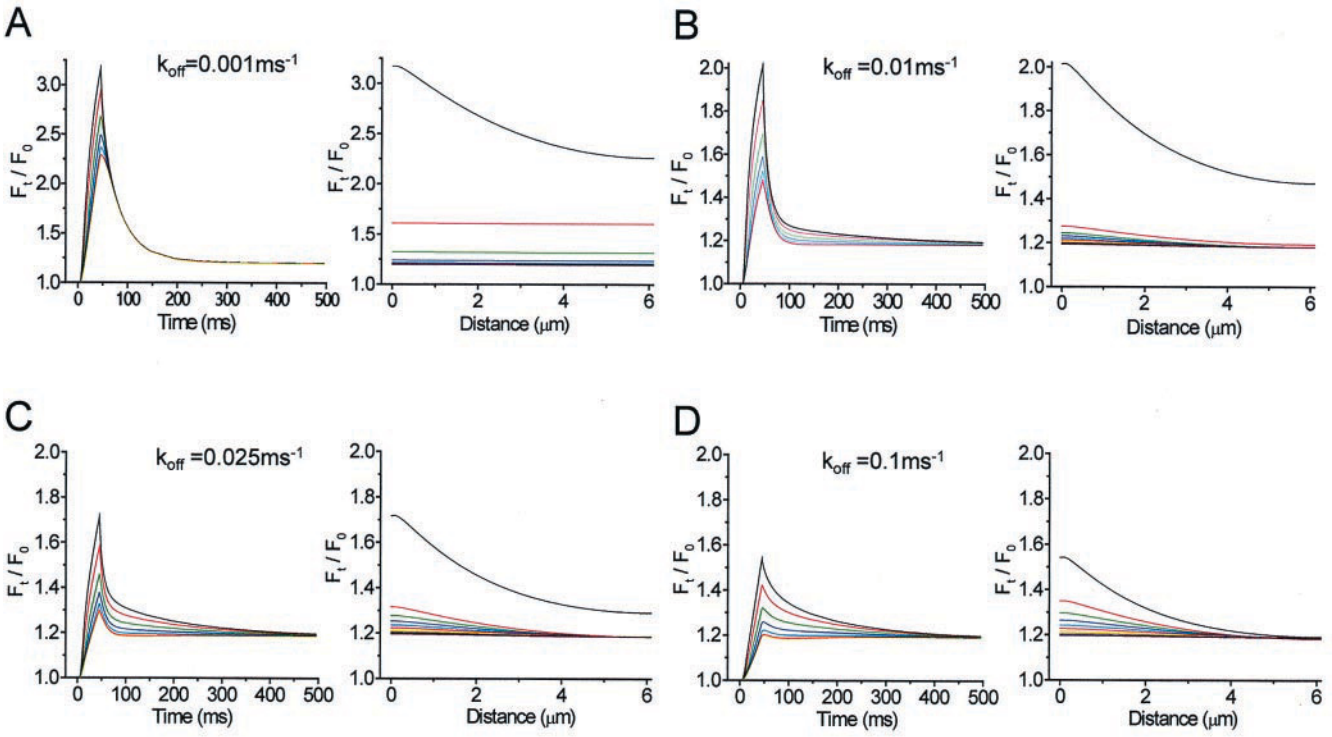

FIGURE 7 Simulation of Ca^{2+}gradients in the presence of high-capacity immobile endogenous Ca^{2+} buffers with different kinetic rate constants. (*A–D*) Simulations of the rhod-2 fluorescence ratio in response to Ca^{2+} entry during a 40-ms depolarizing pulse in the presence of a high-capacity immobile endogenous Ca^{2+} buffer with different kinetic rate constants. As in Fig. 6, the left panel shows the time course and the right panel the profiles through the cell center. In each simulation, the buffer concentration was 1.21mM, and the K_d was 1 μM ($\kappa = 1000$). The kinetic constants were as follows: (*A*) $k_{off} = 0.001$ ms^{-1} and $k_{on} = 1$ mM^{-1}·ms^{-1}; (*B*) $k_{off} = 0.01$ ms^{-1} and $k_{on} = 10$ mM^{-1}·ms^{-1}; (*C*) $k_{off} = 0.025$ ms^{-1} and $k_{on} = 25$ mM^{-1}·ms^{-1}; (*D*) $k_{off} = 0.1$ ms^{-1} and $k_{on} = 100$ mM^{-1}·ms^{-1}.

slowly when the dissociation rate constant is smaller and Ca^{2+} is released from the buffer more slowly. Close examination of Fig. 7 also shows that with slow endogenous buffer, the edge gradient dissipates rapidly, leaving a shallow gradient that dissipates slowly. This trend can also be seen in the analysis of the edge-center gradient dissipation (Table 2), which shows that the relative size of the slow exponential, A_2, tends to decrease as the k_{off} is reduced. In the extreme case, such as when the rate constants are $k_{off} = 0.001$ ms^{-1} and $k_{on} = 1$ mM^{-1}·ms^{-1} (Fig. 7 *A*), A_2 tends to zero, leaving only the fast component of dissipation. As a result, the gradients dissipate very rapidly ($\tau = 7.4$ ms; Table 2, simulation l). Fig. 7 *A* also shows that the predicted fluorescence changes with such a buffer are three times larger than those measured, suggesting that Ca^{2+} binding to an endogenous buffer with these properties would be too slow to have a significant influence on Ca^{2+} handling.

When the dissociation rate constant of the immobile endogenous buffer is 0.01 ms^{-1} or faster, buffers with a high capacity ($\kappa > 500$) always result in Ca^{2+} gradients that persist for hundreds of milliseconds. Fig. 7 *B* shows a simulation using a buffer with a k_{on} of 10 mM^{-1}·ms^{-1} and a k_{off} of 0.01 ms^{-1} that gave a dissipation time constant (τ_2) of 200 ms, whereas a faster buffer with a k_{on} of 100 mM^{-1}·ms^{-1} and a k_{off} of 0.1 ms^{-1} (Fig. 7 *D*) gave a τ_2 of 125 ms (Table 2). However, increasing k_{off} further did not significantly shorten the dissipation times, as τ_2 tends to plateau at a value that depends on the buffer capacity (e.g., at ~120 ms for $\kappa = 1000$). The explanation for this is that, with these fast buffers, the association rate constant is also larger (to keep the same K_d), with the result that Ca^{2+} is recaptured very rapidly, preventing Ca^{2+} from diffusing very far or binding to mobile Ca^{2+} buffers. Simulations show that, in the presence of such fast buffers, the size of the fluorescence changes becomes small and the Ca^{2+} keeps increasing at the center of the cell for hundreds of milliseconds after the end of the pulse. These characteristics are clearly not consistent with the experimentally measured Ca^{2+} gradients.

The k_{off} values that best approximate our experimental results appear to be between 0.01 and 0.1 ms^{-1} (Fig. 7, *B* and *D*). With k_{off} values at either end of this range, shallow gradients were found to persist over hundreds of milliseconds, but neither perfectly match the measured gradients. With $k_{off} = 0.01$ ms^{-1}, the sharp Ca^{2+} gradient near the edge of the cell dropped too quickly (Fig. 7 *B*), whereas it persisted too long when $k_{off} = 0.1$ ms^{-1} (Fig. 7 *D*). Moreover, in the latter case, the signal at the end of the Ca^{2+}

entry is markedly smaller than the signal in the experiments. A buffer with intermediate kinetic constants, such as $k_{off} = 0.025\ ms^{-1}$ and $k_{on} = 25\ mM^{-1}{\cdot}ms^{-1}$ or $k_{off} = 0.05\ ms^{-1}$ and $k_{on} = 50\ mM^{-1}{\cdot}ms^{-1}$ (Figs. 7 *C* and 6 *C*, Table 2), gives a better balance of the pattern of Ca^{2+} gradient dissipation.

A similar analysis of simulated Ca^{2+} gradients using K_d values for immobile endogenous buffers ranging from 0.1 to 100 μM also showed that buffers with k_{off} values in the range of 0.01–0.1 ms^{-1} best approximate the measured Ca^{2+} gradients (unpublished data; see the WWW Supplement). Within this range, slower dissociation rate constants result in slower dissipation times. For all K_d values, the best simulations were obtained with buffer values in the middle of this range, for example, $k_{off} = 0.025\ ms^{-1}$ or $k_{off} = 0.05\ ms^{-1}$.

We also considered how the values of other parameters used in the simulations could influence our conclusions about endogenous buffer and the observed Ca^{2+} gradients. We ran a large number of simulations where we changed the affinities, rate constants, and diffusion coefficients of the exogenous buffers (Ca^{2+} indicator and EGTA), to explore how errors in the published values might affect our conclusions. We were unable to adequately simulate the sizes of the fluorescence changes, the pattern of gradient development, and the slow gradient dissipation without including a high-capacity immobile buffer. By changing some of the parameters we could match the dissipation time alone, but not the other observed properties. For example, we considered that a slower diffusion coefficient for Ca^{2+} ions and the exogenous mobile Ca^{2+} buffers could result in slow dissipation of the Ca^{2+} gradient with lower endogenous buffer capacities. As expected, simulations with slower diffusion coefficients resulted in slow dissipation times at lower buffer capacities (unpublished data; see the WWW Supplement). For instance, a buffer with $D = 10\ \mu m^2{\cdot}s^{-1}$ (instead of 200 $\mu m^2{\cdot}s^{-1}$) at a buffer capacity of 100 gave a dissipation time of 154 ms (Table 2, simulation t). However, the fluorescence changes were four times larger than those measured (see Table 2), and the fluorescence in the center of the cell continued to increase for hundreds of milliseconds after the depolarizing pulse (unpublished data; see the WWW Supplement), which was not observed with the measured gradients. Reducing the diffusion coefficient by a factor of 2 to $D = 100\ \mu m^2{\cdot}s^{-1}$ slowed gradient dissipation slightly, so the buffer capacity needed to explain the measured gradients is reduced to ~800 (Table 2, simulation r). This simulation gave the best overall fit of the two time constants and relative magnitudes of the two components of fluorescence gradient dissipation, and of the size of the fluorescence changes. Based on our simulations, we propose that the sizes of the measured fluorescence changes and the persistence of Ca^{2+} gradients for hundreds of milliseconds are best explained by the presence of an immobile high-capacity endogenous Ca^{2+} buffer.

Measurement of Ca^{2+} gradients with a low-affinity Ca^{2+} indicator dye

Rhod-2 is a medium-affinity dye, which binds significant amounts of Ca^{2+}, reducing the size of the Ca^{2+} changes. In addition, because of its relatively slow kinetics ($k_{off} = 0.13\ ms^{-1}$), this indicator may not accurately measure fast Ca^{2+} changes near the plasma membrane. In contrast, a lower affinity (and faster) indicator dye, such as Oregon Green BAPTA-5N (OGB-5N), may have a less perturbing effect and more accurately detect rapid Ca^{2+} changes (Escobar et al., 1994; DiGregorio and Vergara, 1997).

Fig. 8 shows the development of Ca^{2+} gradients measured with OGB-5N. The profiles of F_t/F_o and the Ca^{2+} concentration change estimated from the fluorescence measurements are shown in Fig. 8, *A* and *B*, respectively. For comparison, the corresponding measurements with rhod-2 are shown in Fig. 8, *E* and *F*. The measured Ca^{2+} gradient appears sharper, as the increase at the edge of the cell is larger with OGB-5N and the spread of Ca^{2+} toward the center of the cell is slower (compare Fig. 8 *B* with Fig. 8 *F*). The space constants measured from half-profiles at 40 ms were $1.92 \pm 0.21\ \mu m$ for OGB-5N and $2.69 \pm 0.24\ \mu m$ for rhod-2 ($p < 0.05$), respectively.

Fig. 8, *C* and *D*, shows model simulations using OGB-5N as the indicator with and without compensation for out-of-focus light due to the blurring effect of the microscope optics (see Materials and Methods). Comparison of the two simulations clearly shows how out-of-focus light affects the shape of the Ca^{2+} gradient, so that it appears less sharp and better represents the experimental data. In addition, without the blurring there is no increase in the center of the cell with OGB-5N (Fig. 8 *D*), indicating that the increase in fluorescence at the cell center is due to out-of-focus light. In contrast, with rhod-2 the increase in fluorescence at the center of the cell also includes a component due to a Ca^{2+} increase (Fig. 8, *G* and *H*). The Ca^{2+} gradients measured with rhod-2 and OGB-5N are different because the time that Ca^{2+} takes to diffuse to the center of the cell is dependent on both fixed and mobile buffers (Nowycky and Pinter, 1993). Ca^{2+} binding to immobile endogenous buffer slows the movement of Ca^{2+}, whereas binding to mobile buffer, which competes with the immobile buffer, facilitates the net movement of Ca^{2+} toward the cell center. This increased movement of Ca^{2+} toward the center is dependent on the concentration and affinity of the mobile buffer. The higher Ca^{2+} affinity and relatively slow k_{off} of rhod-2 ensure that more Ca^{2+} remains bound and more Ca^{2+} is carried to the cell center than with the low-affinity indicator.

When measuring the dissipation of the Ca^{2+} gradients with OGB-5N, we found that a gradient was detectable 60 and 160 ms after the end of the stimulus (unpublished data). However, it was difficult to determine whether shallow gradients were present at later times because of the low signal-to-noise ratio with OGB-5N. This is due, in part, to

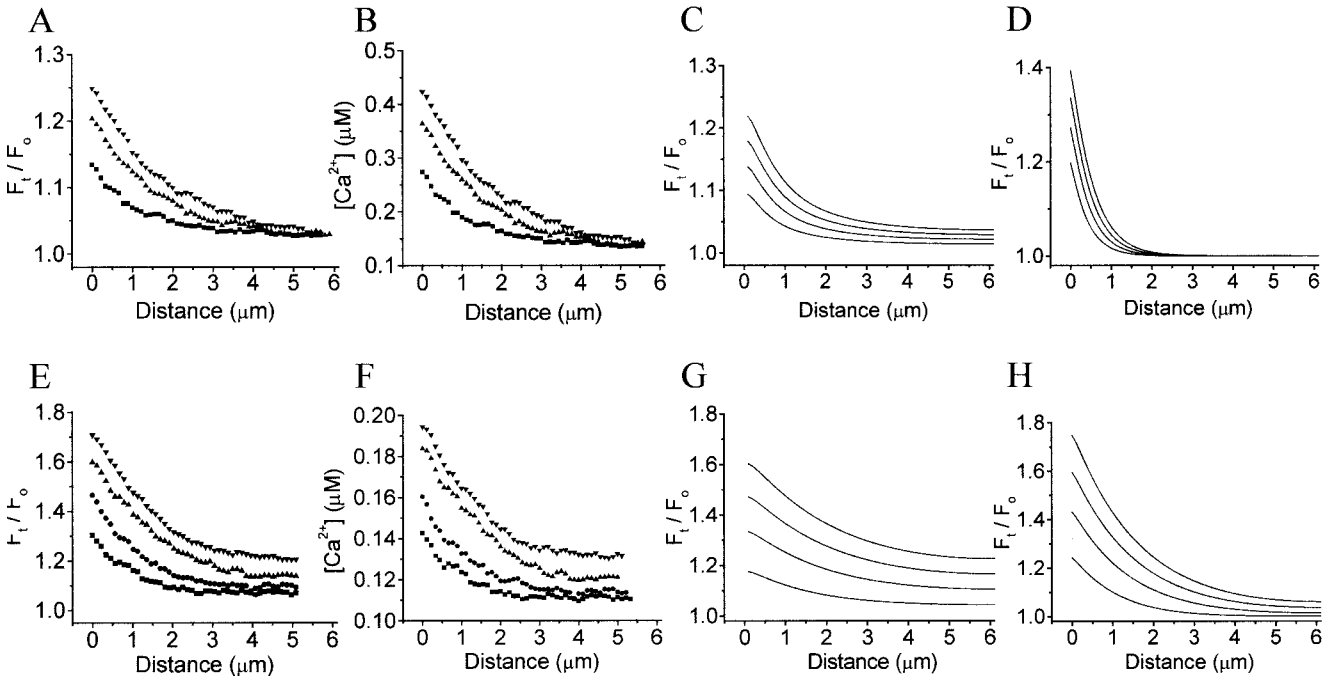

FIGURE 8 Comparison of Ca^{2+}gradients measured with rhod-2 and OGB-5N. (*A*) Half-profiles of F_t/F_o values, showing the development of Ca^{2+} gradients measured with OGB-5N. (*B*) Half-profiles of the Ca^{2+} concentration estimated from the F_t/F_o measurements shown in *A*. (*E* and *F*) The corresponding F_t/F_o and $[Ca^{2+}]$ measurements with rhod-2 are shown for comparison. The gradients shown were captured 10 (■), 20 (●), 30 (▲), and 40 (▼) ms after the Ca^{2+} channel was induced to open. (*C* and *G*) Simulations with OGB-5N and rhod-2, respectively, using the full radial diffusion model with optical blurring to estimate the observed fluorescence changes. Buffer parameters were the same as in Fig. 6 *C*: $K_d = 1\ \mu M$, $k_{on} = 50\ mM^{-1}{\cdot}ms^{-1}$, $k_{off} = 0.05\ ms^{-1}$. The endogenous buffer concentration used for rhod-2 simulations was 1.21 mM ($\kappa = 1000$), whereas for OGB-5N the concentration was reduced to 0.605 mM ($\kappa = 500$) to better approximate the size of the experimental fluorescence changes. (D and H) Simulations with OGB-5N and rhod-2, respectively, using the radial diffusion model without the optical blurring.

the very small amounts of Ca^{2+} bound to the indicator as a result of its low affinity. In addition, the fluorescence ratio (S_b/S_f) of the Ca^{2+}-saturated indicator and free indicator is smaller for OGB-5N (25 versus 77 for OGB-5N and rhod-2, respectively). Our simulations predict that the Ca^{2+} gradient is maintained longer in the presence of OGB-5N than with rhod-2, although the gradient of the F_t/F_o signal becomes very shallow after the stimulus. These findings are important to consider when choosing Ca^{2+} indicators. Ideally, OGB-5N is less perturbing and would be the indicator of choice, but for small Ca^{2+} changes it would not be sensitive enough and rhod-2 would therefore be a more practical choice. However, for fast, localized changes OGB-5N has clear advantages as an indicator (e.g., see DiGregorio and Vergara, 1997; DiGregorio et al., 1999).

DISCUSSION

In this study we measured Ca^{2+} gradients in adrenal chromaffin cells at high temporal and spatial resolution under different experimental conditions, using a pulsed laser imaging system (Monck et al., 1994). This represents the first detailed characterization of the development and dissipation of Ca^{2+} gradients induced by Ca^{2+} entry. By comparing the measured Ca^{2+} gradients with those predicted by simulation with a radial diffusion model, we were able to characterize the properties of a high-capacity immobile endogenous buffer in the cytosol of adrenal chromaffin cells.

Development and dissipation of Ca^{2+} gradients

Stimulation of Ca^{2+} channel opening in adrenal chromaffin cells by short depolarizing stimuli (40 ms) led to the development of Ca^{2+} gradients (Figs. 1 and 2). At early times ($<$10 ms) the Ca^{2+} increase was restricted to the submembrane region, and after 20–30 ms Ca^{2+} also increased at the center of the cell. Estimates of the amount of Ca^{2+} entering the cell (calculated from the Ca^{2+} current) and of the free Ca^{2+} concentration (fluorescence of indicator) indicate that only a small fraction of the Ca^{2+} entering the cell remains free in the cytosol ($<$0.1%). These data, together with our simulations (Figs. 6 and 7, Table 2), suggest that there must be an endogenous Ca^{2+} buffer with a high capacity, on the order of 1000, in addition to the exogenous Ca^{2+} buffers added with the pipette solution.

After the depolarizing stimulus the Ca^{2+} gradient dissipates over several hundred milliseconds to leave a uniformly elevated Ca^{2+} concentration (Fig. 3), which decays

to rest over several seconds. Measurements of the Ca^{2+} gradients show that immediately after the end of the pulse the Ca^{2+} concentration starts to decrease at the cell periphery, whereas it continues to increase at the center of the cell as Ca^{2+} redistributes because of diffusion (Figs. 3 and 4). The Ca^{2+} gradients persist for more than 400 ms after the end of the depolarizing pulse (Figs. 3–5). Similar persistence of Ca^{2+} gradients for hundreds of milliseconds after a depolarizing stimulus has been observed in previous studies (Monck et al., 1994; Naraghi et al., 1998).

Possible contribution of intracellular Ca^{2+} transport to cytosolic Ca^{2+} buffering

We tested the hypothesis that Ca^{2+} uptake by intracellular stores, such as endoplasmic reticulum or mitochondria, could contribute significantly to the buffer capacity of the cytoplasm. We found that thapsigargin, an inhibitor of the endoplasmic reticulum Ca^{2+}-ATPase, did not affect the size of the Ca^{2+} changes during or after the pulse, and the time needed for complete dissipation of the Ca^{2+} gradient was not significantly changed (Fig. 5). Similarly, mitochondrial inhibitors (FCCP plus oligomycin) did not significantly affect the time course of Ca^{2+} gradient dissipation after the pulse (Fig. 5). These results show that, under our conditions, Ca^{2+} transport by the major intracellular Ca^{2+} stores does not play a major role in cytosolic Ca^{2+} redistribution during Ca^{2+} gradient development and dissipation. However, this does not rule out Ca^{2+} uptake by other intracellular organelles such as chromaffin granules by an unknown mechanism.

After Ca^{2+} gradient dissipation, the cytosolic Ca^{2+} concentration remains uniformly elevated and returns slowly to resting levels. Uncoupling the mitochondria slowed down the return of average Ca^{2+} to resting levels (Fig. 5 *B*). This is consistent with the results of Herrington et al. (1996), who found that Ca^{2+} clearance after Ca^{2+} entry in rat adrenal chromaffin cells was slowed by the treatment with mitochondrial uncoupler. However, the slower clearance in our experiments could simply be due to the smaller Ca^{2+} increase that occurred in the presence of mitochondrial inhibitors. In contrast, inhibition of the endoplasmic reticulum Ca^{2+}-ATPase (Fig. 5) or inhibition of Na/Ca exchange had no significant effect on Ca^{2+} clearance over 500 ms. Nevertheless, because our experiments were carried out over a relatively short period of time (500 ms), our results do not preclude a role of Na/Ca exchange or uptake into reticular Ca^{2+} stores in the slow recovery of the Ca^{2+} concentration to resting levels. In fact, several studies have shown that reticular Ca^{2+} stores and Na/Ca exchange do play a role in Ca^{2+} clearance in adrenal chromaffin cells (Herrington et al., 1996; Pan and Kao, 1997; Xu et al., 1997; Tang et al., 2000).

Properties of endogenous Ca^{2+} buffers

To account for the properties of the measured Ca^{2+} gradients, we have suggested the presence of a high-capacity endogenous Ca^{2+} buffer. To explore this possibility, we used the radial diffusion model described in Materials and Methods to investigate how endogenous Ca^{2+} buffers affect the development and dissipation of Ca^{2+} gradients. We chose a number of properties of the measured Ca^{2+} gradients as a means of assessing model parameters. The main quantitative properties that we considered were the size of the fluorescence change, F_t/F_o, at the edge of the cell and the rate of Ca^{2+} gradient dissipation after the end of the depolarizing pulse. We also considered the shape of the Ca^{2+} gradients, notably the relatively sharp edge gradients that can be seen up to 100 ms (60 ms after the pulse) and the shallow gradient to the cell center that is seen thereafter. Based on a large number of simulations, we drew a number of conclusions about the properties of the endogenous Ca^{2+} buffer, which will be discussed below.

The endogenous Ca^{2+} buffer should be fixed or poorly mobile for two reasons. First, our Ca^{2+} measurements are made in patch-clamped cells 10 min after the whole-cell mode is established, to allow equilibration of the Ca^{2+} indicator between the pipette and the cytosol. Any highly mobile buffer will diffuse out of the cell under these conditions (Zhou and Neher, 1993). Second, a mobile endogenous buffer will not generate persistent Ca^{2+} gradients, because Ca^{2+} binding to mobile buffers should lead to rapid Ca^{2+} redistribution after the depolarizing pulse. Indeed, our simulations indicate that Ca^{2+} gradients dissipate rapidly when the diffusion coefficient of the endogenous buffer is greater than 10 $\mu m^2 \cdot s^{-1}$ (unpublished data; see the WWW Supplement). Thus, as previously suggested, rapid gradient dissipation is very likely due to mobile Ca^{2+} buffers carrying Ca^{2+} toward the cell center (Nowycky and Pinter, 1993). As a corollary, the endogenous buffer must be relatively immobile to prolong the Ca^{2+} gradients.

The endogenous Ca^{2+} buffer should have a high capacity to capture a significant fraction of the Ca^{2+} entering the cell and to compete efficiently with the mobile exogenous buffers. As shown in Fig. 6 and Table 2, buffers with K_d values between 1 and 100 μM must have a buffer capacity of $\sim$1000 to obtain reasonable approximations of the F_t/F_o values and of the time for Ca^{2+} gradient dissipation. The dissipation times for buffers with K_d values of 1, 10, and 100 μM (k_{off} = 0.05 ms^{-1}) are 129, 150, and 152 ms, respectively, within the 95% confidence range of the measured dissipation time (114–218 ms). For a buffer with a 1 μM K_d and k_{off} = 0.05 ms^{-1}, the buffer capacities giving dissipation times that match the upper and lower confidence limits are in the range of 870-1800. For higher affinity buffers the buffer capacity must be higher (e.g., 1250–2400 for K_d = 0.1 μM), and for lower affinity buffers the required capacity is slightly lower (e.g., 720-1540 for K_d = 10

μM). In all cases (affinities and kinetics), the buffer capacity must be at least 700 to match the lower range of the measured dissipation time.

These estimates of the endogenous fixed buffer capacity are significantly larger than previous estimates (31–90) for adrenal chromaffin cells (Neher and Augustine, 1992; Zhou and Neher, 1993). Using such a low-capacity endogenous buffer (4 mM of a low-affinity buffer (K_d = 100 μM) with the kinetic rate constants from Xu et al. (1997)), we found that simulated Ca^{2+} gradients have considerably larger Ca^{2+} increases (more than threefold) and that the gradients dissipate an order of magnitude faster (τ = 14 ms; Table 2, simulation b) than the measured Ca^{2+} gradients. These simulated gradients are similar to those shown in Fig. 6 *A* for a buffer capacity of 100, which resulted in a fluorescence gradient that dissipated with a time constant of 28 ms. The simulations in Fig. 6 clearly demonstrate that a buffer with a higher endogenous buffer capacity is necessary to account for the properties of the measured Ca^{2+} gradients.

Previous studies have developed a steady-state buffer theory to devise methods to estimate endogenous Ca^{2+} buffer capacity (Neher and Augustine, 1992; Zhou and Neher, 1993). These methods rely on the competition between the indicator (exogenous buffer) and endogenous buffer at different indictor concentrations. A number of assumptions regarding spatial equilibrium of Ca^{2+} and mobile Ca^{2+} buffers and kinetic equilibrium of Ca^{2+} with all Ca^{2+} buffers were necessary to derive the equations used to calculate Ca^{2+} buffer capacity. The methods also assume that the increments in Ca^{2+} concentration are small and that cellular Ca^{2+} clearance mechanisms act linearly with Ca^{2+} concentration. However, if the system is not at kinetic and spatial equilibrium, as will be the case while Ca^{2+} gradients are present, these methods will underestimate the buffer capacity for the following reason. When Ca^{2+} enters the cell it binds either endogenous immobile buffer or mobile Ca^{2+} indicator. Most of the Ca^{2+} bound to the endogenous immobile buffer is near the cell membrane, whereas the Ca^{2+} bound to mobile indicator is measured from the whole cell. As a result, if the system is not at spatial equilibrium, the endogenous buffer in the center of the cell does not contribute to the apparent buffering. To explore this effect, we simulated Ca^{2+} gradients and found that significant gradients of Ca^{2+}-bound endogenous buffer complex persist long after a short (40 ms) depolarization, especially at low exogenous buffer capacities (e.g., $<$50 μM fura-2), when the gradients of Ca^{2+}-endogenous buffer complex persist for several seconds. Therefore, the assumption of kinetic equilibrium in a single compartment may not be valid until several seconds after the end of the stimulus. This will lead to underestimation of buffer capacities calculated by extrapolation of Ca^{2+} clearance time constants to zero exogenous buffer (Neher and Augustine, 1992). It will also underestimate buffer capacities calculated from the relative amounts of Ca^{2+} captured by indicator at different indicator concentrations (Neher and Augustine, 1992; Zhou and Neher, 1993), because the fluorescence change measured immediately after the depolarizing pulse will overestimate the relative amount of Ca^{2+} captured by the indicator when the system is not at spatial equilibrium.

Our work takes a very different approach that does not require us to make any assumptions about spatial and kinetic equilibrium. Instead, we measure the kinetics and spatial inhomogeneity of the Ca^{2+} increase after Ca^{2+} entry through Ca^{2+} channels, and compare these Ca^{2+} gradients with gradients simulated with a mathematical diffusion model. The assumptions required for this approach are implicit in the geometry of the model and the values of the parameters used. The model assumes an even distribution of endogenous buffer in the cytoplasm, which appears reasonable, given the lack of inflections in the shallow gradients measured during dissipation (200–500 ms; see Fig. 4). The values used for the kinetic properties of the exogenous buffers have been reported in the literature (see references in Table 1) and have been used in many previous modeling studies (see Sala and Hernández-Cruz, 1990; Nowycky and Pinter, 1993; Klingauf and Neher, 1997). As described in the Results, we have carried out a large number of simulations to explore the sensitivity of our endogenous buffer capacity estimates to the values of these parameters and found no other way of satisfactorily reproducing the properties of the measured Ca^{2+} gradients.

We tried to estimate the affinity and kinetic constants of the endogenous Ca^{2+} buffer by comparing the dissipation times and the size and shape of measured and simulated Ca^{2+} gradients. Thus we were able to determine that the dissociation rate constant needs to be in the range of 0.01–0.1 ms^{-1} (see Results), but we could not definitely assess the affinity of the endogenous buffer. At appropriately high buffer capacities, K_d values in the range 0.1–100 μM gave satisfactory approximation of the data. However, whereas a buffer with a K_d of 1 μM would have to be present at 1.21 mM binding sites to give a buffer capacity of 1000, lower affinity buffers with K_d values of 10 μM and 100 μM would have to be present at 10.2 mM and 100.2 mM, respectively (Table 2). These are very high concentrations for a protein, so it seems improbable that a Ca^{2+}-binding protein with a K_d greater than 10 μM could be present at a sufficient concentration to account for the required buffer capacity. On the other hand, a high-affinity buffer with a K_d of 0.1 μM would have to be present at a buffer capacity of 1500 to give an appropriate dissipation time (Table 2), requiring 0.61 mM binding sites.

The above analysis used a radial diffusion model that incorporates three-dimensional optical sectioning to simulate the effects of out-of-focus light, to allow direct comparison with the experimental data (see Materials and Methods). Initially, we carried out the analysis using the basic radial diffusion model (Nowycky and Pinter, 1993) without accounting for the optical properties of the microscope and

came to very similar conclusions (unpublished data; see the WWW Supplement). The conclusions regarding the K_d and k_{off} of the endogenous buffer were identical, but the estimates for the buffer capacity were ~20–30% lower.

It should be noted that a simple radial diffusion model ignores several factors that are likely to be true of real cells. Adrenal chromaffin cells are not perfect spheres with a completely homogeneous distribution of Ca^{2+} buffers. Furthermore, there is likely to be a mixture of different Ca^{2+}-binding proteins in the cytosol, with some heterogeneous distribution and possibly some cooperative properties. These proteins may be relatively immobile on the time frame of our experiments, but there might be changes in distribution of Ca^{2+} buffers or changes in their Ca^{2+} binding properties under certain circumstances, which might occur during stimulation of cells with repetitive stimuli. Therefore, it should be emphasized that we are drawing general conclusions about the characteristics of the cytoplasmic Ca^{2+} buffers that we think are necessary to explain the properties of the measured Ca^{2+} gradients; we are not trying to give a precise estimate of the concentration, K_d, or rate constants of any specific endogenous Ca^{2+} buffer.

Physiological considerations involving Ca^{2+}-binding proteins

The family of Ca^{2+}-binding proteins containing an E-F hand motif is now known to comprise more than 200 members (Heizmann, 1992). Several of these proteins, including calmodulin, calbindin-D28K (or neuronal Ca sensor 1), and calretinin, have been identified in adrenal chromaffin cells (Afework and Burnstock, 1995; Buffa et al., 1989; Hikita et al., 1984; McFerran et al., 1998). A significant proportion was found to be associated with intracellular membrane fractions (Hikita et al., 1984; Winsky and Kuznicki, 1995; McFerran et al., 1998) and would be expected to be relatively immobile. These proteins typically have a K_d for Ca^{2+} of 0.5–1 μM in physiological solutions (Linse et al., 1991; Chard et al., 1993; Martin et al., 1990; Bredderman and Wasserman, 1974; McFerran et al., 1998; Schwaller et al., 1997; Stevens and Rogers, 1997). Another type of Ca^{2+}-binding protein is the annexin family, several members of which (types I, II, IV, V, VI, and VII) have been found in adrenal chromaffin cells (Drust and Creutz, 1991; Burgoyne and Geisow, 1989). A large fraction of these proteins were associated with membranes. Annexins typically bind Ca^{2+} with K_d values of 1–10 μM in the presence of phospholipids (Jost et al., 1992; Thiel et al., 1991; Drust and Creutz, 1991; Burgoyne and Geisow, 1989)

Most of the Ca^{2+}-binding proteins reported in adrenal chromaffin cells have a K_d on the order of 1 μM. Although regulatory proteins such as calmodulin are present at concentrations of a few μM (Stevens and Rogers, 1997; Hikita et al., 1984), some of the annexins and calbindin-D28K may be present at higher concentrations. Calbindin-D28K, for instance, is present in the basilar papilla of chicken cochlea at concentrations in excess of 1 mM (Oberholtzer et al., 1988) and in cerebellar Purkinje neurons at more than 0.1 mM (Baimbridge et al., 1982). Buffer capacities as high as 900-2000 have been measured in Purkinje neurons (Fierro and Llano, 1996). For calbindin-D28K to contribute a buffer capacity of 1000, it would have to be present in adrenal chromaffin cells at 180–120 μM, assuming four to six functional Ca^{2+} binding sites per molecule (Bredderman and Wasserman, 1974; Leathers et al., 1990), a K_d in physiological $[K^+]$ of 0.5 μM (Bredderman and Wasserman, 1974; Leathers et al., 1990), and the same kinetic properties as calbindin-9k, which has an association rate constant of 20 $mM^{-1}{\cdot}ms^{-1}$ and a dissociation rate constant on the order of 0.01 ms^{-1} (Martin et al., 1990).

Physiological consequences

The pattern of Ca^{2+} gradient is strongly influenced by the properties of the Ca^{2+} buffers. We have already discussed how the properties of the endogenous immobile Ca^{2+} buffer can have profound effects on the temporal and spatial patterns of Ca^{2+} gradients. It is equally true that the exogenous mobile Ca^{2+} buffers used as Ca^{2+} indicators affect the properties of the Ca^{2+} gradients, as illustrated by the different Ca^{2+} gradients found with rhod-2 and OGB-5N (Fig. 8). The next logical step is to find out what the Ca^{2+} gradient would look like under physiological conditions in the absence of exogenous Ca^{2+} buffers.

Fig. 9 shows the Ca^{2+} gradients predicted by simulations using no exogenous mobile Ca^{2+} buffer, but only an immobile endogenous Ca^{2+} buffer with the characteristics that we have determined: concentration 1.21 mM, K_d = 1 μM, k_{on} = 50 $mM^{-1}{\cdot}ms^{-1}$, k_{off} = 0.05 ms^{-1}, and κ = 1000. Several features of the simulated Ca^{2+} gradients deserve comment. First, the gradient develops very fast during the first 5–10 ms and is limited by the rate of Ca^{2+} channel activation. The Ca^{2+} concentration in the outer 100-nm shell reaches a concentration of ~500 nM after ~10 ms. Second, a Ca^{2+} gradient persists for a long time after Ca^{2+} channel closure. In this simulation, the gradient dissipation takes more than 10 s. However, there is likely to be some mobile endogenous buffer in adrenal chromaffin cells, which would lead to faster dissipation. In fact, Zhou and Neher (1993) have estimated that 25% of the endogenous buffer might be mobile and wash out of chromaffin cells under whole-cell recording conditions. Therefore, under physiological conditions dissipation of the Ca^{2+} gradients is likely to be controlled by endogenous mobile Ca^{2+} buffers and Ca^{2+} clearance mechanisms. Third, the Ca^{2+} gradient is restricted to a region less than 1 μm from the cell membrane. Thus, high-capacity immobile Ca^{2+} buffers restrict the Ca^{2+} change to within ~1 μm from the site of Ca^{2+} entry. As a result, for a depolarizing stimulus to cause a Ca^{2+} elevation elsewhere in the cell, other mechanisms

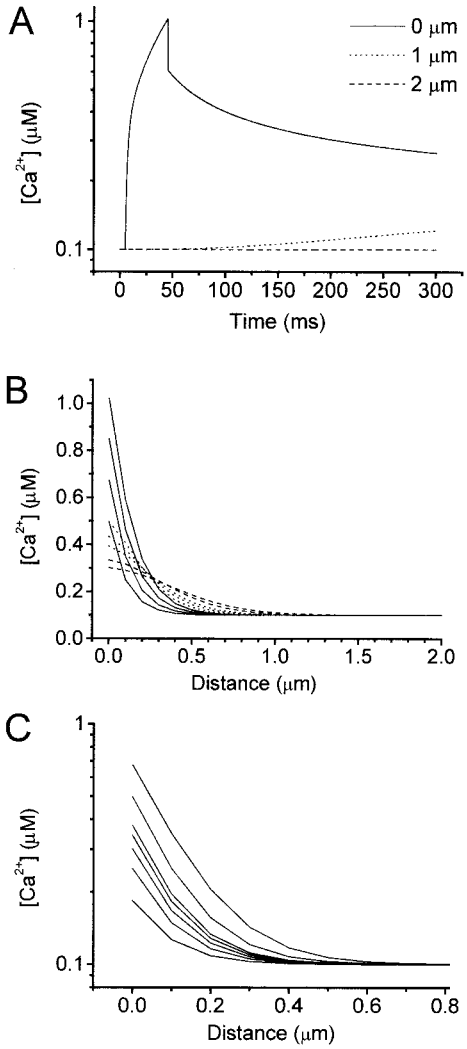

FIGURE 9 Simulation of Ca^{2+} gradients predicted to occur in the absence of Ca^{2+} indicators. Ca^{2+} gradients were simulated in the absence of exogenous Ca^{2+} buffers (indicator and EGTA), using the following parameters for the immobile Ca^{2+} buffer (same as in Fig. 6 *C*): K_d = 1 μM, k_{on} = 50 $mM^{-1}{\cdot}ms^{-1}$, k_{off} = 0.05 ms^{-1}, concentration = 1.21 mM (κ = 1000). (*A*) The Ca^{2+} concentration time courses for the shells nearest the plasma membrane (0 μm) and 1 and 2 μm from the membrane. The values for shells at 3–6 μm are not shown because they superimposed on the values for the shell at 2 μm. (*B*) Half-profiles of the Ca^{2+} gradients taken during (*solid lines*, 10, 20, 30, 40 ms) and after (*broken lines,* 60, 80, 100, 150, 200 ms) Ca^{2+} entry. (*C*) Half-profiles of the Ca^{2+} gradients at high time resolution during Ca^{2+} entry (1, 2, 3, 4, 5, 10, 20 ms).

such as propagating intracellular Ca^{2+} release mechanisms or mobile buffers must participate.

Finally, it is important to consider that the properties of the Ca^{2+} gradients in small cells are strongly influenced by the Ca^{2+} indicator (compare Fig. 8 *B* and Fig. 8 *F*) and by the presence of exogenous buffers (Fig. 9). Thus in studies of the regulation of exocytosis by Ca^{2+} it would be highly advantageous to measure Ca^{2+} gradients and exocytosis simultaneously in the same cell. How Ca^{2+} gradients change during repetitive stimulation and how these affect rapid and slow phases of exocytosis and facilitation will be the subject of future studies.

We thank Drs. Julio Vergara and David DiGregorio for many interesting discussions on cellular Ca^{2+} buffering, Ca^{2+} measurements, and modeling of the Ca^{2+} gradients. Special thanks are due to Dr. Bernard Ribalet for critical reading of the manuscript and Dr. Art Peskoff for valuable insight into the mathematical modeling.

This work was supported by grant GM54340 (to JRM) from the National Institutes of Health.

REFERENCES

Afework, M., and G. Burnstock. 1995. Calretinin immunoreactivity in adrenal glands of developing, adult and ageing Sprague-Dawley rats. *Int. J. Dev. Neurosci.* 13:515–521.

Allbritton, N. L., T. Meyer, and L. Stryer. 1992. Range of messenger action of calcium ion and inositol 1,4,5-trisphosphate. *Science.* 258: 1812–1815.

Augustine, G. J., and E. Neher. 1992. Calcium requirements for secretion in bovine chromaffin cells. *J. Physiol. (Lond.).* 450:247–271.

Baimbridge, K. G., J. J. Miller, and C. O. Parkes. 1982. Calcium-binding protein distribution in the rat brain. *Brain Res.* 239:519–525.

Bredderman, P. J., and R. H. Wasserman. 1974. Chemical composition, affinity for calcium, and some related properties of the vitamin D dependent calcium-binding protein. *Biochemistry.* 13:1687–1694.

Bright, G. R., G. W. Fisher, J. Rogowska, and D. L. Taylor. 1989. Fluorescence ratio imaging microscopy. *Methods Cell Biol.* 30:157–192.

Buffa, R., P. Mare, M. Salvadore, E. Solcia, J. B. Furness, and D. E. Lawson. 1989. Calbindin 28 kDa in endocrine cells of known or putative calcium-regulating function. Thyro-parathyroid C cells, gastric ECL cells, intestinal secretin and enteroglucagon cells, pancreatic glucagon, insulin and PP cells, adrenal medullary NA cells and some pituitary (TSH?) cells. *Histochemistry.* 91:107–113.

Burgoyne, R. D., and M. J. Geisow. 1989. The annexin family of calcium-binding proteins. Review article. *Cell Calcium.* 10:1–10.

Burgoyne, R. D., A. Morgan, and A. J. O'Sullivan. 1988. A major role for protein kinase C in calcium-activated exocytosis in permeabilised adrenal chromaffin cells. *FEBS Lett.* 238:151–155.

Chad, J. E., and R. Eckert. 1984. Calcium domains associated with individual channels can account for anomalous voltage relations of CA-dependent responses. *Biophys. J.* 45:993–999.

Chard, P. S., D. Bleakman, S. Christakos, C. S. Fullmer, and R. J. Miller. 1993. Calcium buffering properties of calbindin D28k and parvalbumin in rat sensory neurones. *J. Physiol. (Lond.).* 472:341–357.

Connor, J. A., and G. Nikolakapoulou. 1982. Calcium diffusion and buffering in nerve cytoplasm. *Lect. Math. Life Sci.* 15:79–101.

Crank, J. 1975. The Mathematics of Diffusion. Clarendon Press, Oxford.

DiGregorio, D. A., A. Peskoff, and J. L. Vergara. 1999. Measurement of action potential-induced presynaptic calcium domains at a cultured neuromuscular junction. *J. Neurosci.* 19:7846–7859.

DiGregorio, D. A., and J. L. Vergara. 1997. Localized detection of action potential-induced presynaptic calcium transients at a *Xenopus* neuromuscular junction. *J. Physiol. (Lond.).* 505:585–592.

Drust, D. S., and C. E. Creutz. 1991. Differential subcellular distribution of p36 (the heavy chain of calpactin I) and other annexins in the adrenal medulla. *J. Neurochem.* 56:469–478.

Engisch, K. L., and M. C. Nowycky. 1998. Compensatory and excess retrieval: two types of endocytosis following single step depolarizations in bovine adrenal chromaffin cells. *J. Physiol. (Lond.).* 506:591–608.

Escobar, A. L., J. R. Monck, J. M. Fernandez, and J. L. Vergara. 1994. Localization of the site of Ca^{2+} release at the level of a single sarcomere in skeletal muscle fibres. *Nature.* 367:739–741.

Escobar, A. L., P. Velez, A. M. Kim, F. Cifuentes, M. Fill, and J. L. Vergara. 1997. Kinetic properties of DM-nitrophen and calcium indicators: rapid transient response to flash photolysis. *Pflugers Arch.* 434:615–631.

Fierro, L., and I. Llano. 1996. High endogenous calcium buffering in Purkinje cells from rat cerebellar slices. *J. Physiol. (Lond.).* 496: 617–625.

Grynkiewicz, G., M. Poenie, and R. Y. Tsien. 1985. A new generation of Ca^{2+} indicators with greatly improved fluorescence properties. *J. Biol. Chem.* 260:3440–3450.

Hall, J. D., S. Betarbet, and F. Jaramillo. 1997. Endogenous buffers limit the spread of free calcium in hair cells. *Biophys. J.* 73:1243–1252.

Heizmann, C. W. 1992. Calcium-binding proteins: basic concepts and clinical implications. *Gen. Physiol. Biophys.* 11:411–425.

Herrington, J., Y. B. Park, D. F. Babcock, and B. Hille. 1996. Dominant role of mitochondria in clearance of large Ca^{2+} loads from rat adrenal chromaffin cells. *Neuron.* 16:219–228.

Hikita, T., M. F. Bader, and J. M. Trifaró. 1984. Adrenal chromaffin cell calmodulin: its subcellular distribution and binding to chromaffin granule membrane proteins. *J. Neurochem.* 43:1087–1097.

Jost, M., C. Thiel, K. Weber, and V. Gerke. 1992. Mapping of three unique Ca(2+)-binding sites in human annexin II. *Eur. J. Biochem.* 207: 923–930.

Kim, K. T., and E. W. Westhead. 1989. Cellular responses to Ca^{2+} from extracellular and intracellular sources are different as shown by simultaneous measurements of cytosolic Ca^{2+} and secretion from bovine chromaffin cells. *Proc. Natl. Acad. Sci. USA.* 86:9881–9885.

Kinosita, K., Jr., I. Ashikawa, M. Hibino, M. Shigemori, H. Yoshimura, H. Itoh, K. Nagayama, and A. Ikegami. 1988. Submicrosecond imaging under a pulsed-laser fluorescence microscope. *SPIE.* 909:271–277.

Klingauf, J., and E. Neher. 1997. Modeling buffered Ca^{2+} diffusion near the membrane: implications for secretion in neuroendocrine cells. *Biophys. J.* 72:674–690.

Kushmerick, M. J., and R. J. Podolsky. 1969. Ionic mobility in muscle cells. *Science.* 166:1297–1298.

Leathers, V. L., S. Linse, S. Forsén, and A. W. Norman. 1990. Calbindin-D28K, a 1 alpha, 25-dihydroxyvitamin D3-induced calcium-binding protein, binds five or six Ca^{2+} ions with high affinity. *J. Biol. Chem.* 265:9838–9841.

Linse, S., A. Helmersson, and S. Forsén. 1991. Calcium binding to calmodulin and its globular domains. *J. Biol. Chem.* 266:8050–8054.

Martin, S. R., S. Linse, C. Johansson, P. M. Bayley, and S. Forsén. 1990. Protein surface charges and Ca^{2+} binding to individual sites in calbindin D9k: stopped-flow studies. *Biochemistry.* 29:4188–4193.

McFerran, B. W., M. E. Graham, and R. D. Burgoyne. 1998. Neuronal Ca^{2+} sensor 1, the mammalian homologue of frequenin, is expressed in chromaffin and PC12 cells and regulates neurosecretion from dense-core granules. *J. Biol. Chem.* 273:22768–22772.

Minta, A., J. P. Kao, and R. Y. Tsien. 1989. Fluorescent indicators for cytosolic calcium based on rhodamine and fluorescein chromophores. *J. Biol. Chem.* 264:8171–8178.

Monck, J. R., A. F. Oberhauser, T. J. Keating, and J. M. Fernandez. 1992. Thin-section ratiometric Ca^{2+} images obtained by optical sectioning of fura-2 loaded mast cells. *J. Cell Biol.* 116:745–759.

Monck, J. R., E. E. Reynolds, A. P. Thomas, and J. R. Williamson. 1988. Novel kinetics of single cell Ca^{2+} transients in stimulated hepatocytes and A10 cells measured using fura-2 and fluorescent videomicroscopy. *J. Biol. Chem.* 263:4569–4575.

Monck, J. R., I. M. Robinson, A. L. Escobar, J. L. Vergara, and J. M. Fernandez. 1994. Pulsed laser imaging of rapid Ca^{2+} gradients in excitable cells. *Biophys. J.* 67:505–514.

Naraghi, M., T. H. Muller, and E. Neher. 1998. Two-dimensional determination of the cellular Ca^{2+} binding in bovine chromaffin cells. *Biophys. J.* 75:1635–1647.

Neher, E. 1986. Concentration profiles of intracellular calcium in the presence of a diffusible chelator. *Exp. Brain Res. Ser.* 14:980–992.

Neher, E. 1992. Correction for liquid junction potentials in patch clamp experiments. *Methods Enzymol.* 207:123–131.

Neher, E. 1998. Vesicle pools and Ca^{2+} microdomains: new tools for understanding their roles in neurotransmitter release. *Neuron.* 20: 389–399.

Neher, E., and G. J. Augustine. 1992. Calcium gradients and buffers in bovine chromaffin cells. *J. Physiol. (Lond.).* 450:273–301.

Neher, E., and R. S. Zucker. 1993. Multiple calcium-dependent processes related to secretion in bovine chromaffin cells. *Neuron.* 10:21–30.

Nowycky, M. C., and M. J. Pinter. 1993. Time courses of calcium and calcium-bound buffers following calcium influx in a model cell. *Biophys. J.* 64:77–91.

Oberholtzer, J. C., C. Buettger, M. C. Summers, and F. M. Matschinsky. 1988. The 28-kDa calbindin-D is a major calcium-binding protein in the basilar papilla of the chick. *Proc. Natl. Acad. Sci. USA.* 85:3387–3390.

O'Sullivan, A. J., T. R. Cheek, R. B. Moreton, M. J. Berridge, and R. D. Burgoyne. 1989. Localization and heterogeneity of agonist-induced changes in cytosolic calcium concentration in single bovine adrenal chromaffin cells from video imaging of fura-2. *EMBO J.* 8:401–411.

Pan, C. Y., and L. S. Kao. 1997. Catecholamine secretion from bovine adrenal chromaffin cells: the role of the Na^+/Ca^{2+} exchanger and the intracellular Ca^{2+} pool. *J. Neurochem.* 69:1085–1092.

Pusch, M., and E. Neher. 1988. Rates of diffusional exchange between small cells and a measuring patch pipette. *Pflugers Arch.* 411:204–211.

Sala, F., and A. Hernández-Cruz. 1990. Calcium diffusion modeling in a spherical neuron. Relevance of buffering properties. *Biophys. J.* 57: 313–324.

Schwaller, B., I. Durussel, D. Jermann, B. Herrmann, and J. A. Cox. 1997. Comparison of the Ca^{2+}-binding properties of human recombinant calretinin-22k and calretinin. *J. Biol. Chem.* 272:29663–29671.

Seward, E. P., N. I. Chernevskaya, and M. C. Nowycky. 1996. Ba^{2+} ions evoke two kinetically distinct patterns of exocytosis in chromaffin cells, but not in neurohypophysial nerve terminals. *J. Neurosci.* 16: 1370–1379.

Seward, E. P., and M. C. Nowycky. 1996. Kinetics of stimulus-coupled secretion in dialyzed bovine chromaffin cells in response to trains of depolarizing pulses. *J. Neurosci.* 16:553–562.

Simon, S. M., and R. R. Llinás. 1985. Compartmentalization of the submembrane calcium activity during calcium influx and its significance in transmitter release. *Biophys. J.* 48:485–498.

Smith, S. J., and R. S. Zucker. 1980. Aequorin response facilitation and intracellular calcium accumulation in molluscan neurones. *J. Physiol. (Lond.).* 300:167–196.

Stevens, J., and J. H. Rogers. 1997. Chick calretinin: purification, composition, and metal binding activity of native and recombinant forms. *Protein Expr. Purif.* 9:171–181.

Tang, Y. M., E. R. Travis, R. M. Wightman, and A. S. Schneider. 2000. Sodium-calcium exchange affects local calcium signal decay and the rate of exocytotic secretion in single chromaffin cells. *J. Neurochem.* 74:702–710.

Thiel, C., K. Weber, and V. Gerke. 1991. Characterization of a Ca(2+)-binding site in human annexin II by site-directed mutagenesis. *J. Biol. Chem.* 266:14732–14739.

Timmerman, M. P., and C. C. Ashley. 1986. Fura-2 diffusion and its use as an indicator of transient free calcium changes in single striated muscle cells. *FEBS Lett.* 209:1–8.

Winsky, L., and J. Kuznicki. 1995. Distribution of calretinin, calbindin D28k, and parvalbumin in subcellular fractions of rat cerebellum: effects of calcium. *J. Neurochem.* 65:381–388.

Xu, T., M. Naraghi, H. Kang, and E. Neher. 1997. Kinetic studies of Ca^{2+} binding and Ca^{2+} clearance in the cytosol of adrenal chromaffin cells. *Biophys. J.* 73:532–545.

Zhou, Z., and E. Neher. 1993. Mobile and immobile calcium buffers in bovine adrenal chromaffin cells. *J. Physiol. (Lond.).* 469:245–273.

Zucker, R. S., and N. Stockbridge. 1983. Presynaptic calcium diffusion and the time courses of transmitter release and synaptic facilitation at the squid giant synapse. *J. Neurosci.* 3:1263–1269.